Archaeal Signal Transduction: Impact of Protein Phosphatase Deletions on Cell Size, Motility, and Energy Metabolism in *Sulfolobus acidocaldarius**[S]

Julia Reimann‡§§, Dominik Esser§§§, Alvaro Orell‡, Fabian Amman¶, Trong Khoa Pham‖, Josselin Noirel‖, Ann-Christin Lindås, Rolf Bernander**, Phillip C. Wright‖, Bettina Siebers§, and Sonja-Verena Albers‡‡‡**

In this study, the *in vitro* and *in vivo* functions of the only two identified protein phosphatases, Saci-PTP and Saci-PP2A, in the crenarchaeal model organism *Sulfolobus acidocaldarius* were investigated. Biochemical characterization revealed that Saci-PTP is a dual-specific phosphatase (against pSer/pThr and pTyr), whereas Saci-PP2A exhibited specific pSer/pThr activity and inhibition by okadaic acid. Deletion of *saci_pp2a* resulted in pronounced alterations in growth, cell shape and cell size, which could be partially complemented. Transcriptome analysis of the three strains (Δ*saci_ptp*, Δ*saci_pp2a* and the MW001 parental strain) revealed 155 genes that were differentially expressed in the deletion mutants, and showed significant changes in expression of genes encoding the archaella (archaeal motility structure), components of the respiratory chain and transcriptional regulators. Phosphoproteome studies revealed 801 unique phosphoproteins in total, with an increase in identified phosphopeptides in the deletion mutants. Proteins from most functional categories were affected by phosphorylation, including components of the motility system, the respiratory chain, and regulatory proteins. In the *saci_pp2a* deletion mutant the up-regulation at the transcript level, as well as the observed phosphorylation pattern, resembled starvation stress responses. Hypermotility was also observed in the *saci_pp2a* deletion mutant. The results highlight the importance of protein phosphorylation in regulating essential cellular processes in the crenarchaeon *S. acidocaldarius*. ***Molecular & Cellular Proteomics 12: 10.1074/mcp.M113.027375, 3908–3923, 2013.***

Protein phosphorylation is an important post-translational modification (PTM)[1] that has been reported in all three domains of life, Eukarya, Bacteria and Archaea (1–3). The reversible character of the modification allows for subtle and immediate regulation by modulating protein activity in different cellular processes (3–5). The addition of a phosphoryl group is catalyzed by protein kinases and dephosphorylation by their cognate phosphatases. Interestingly, in the Crenarchaeota, one of the phyla of the Archaea, only Ser/Thr/Tyr phosphorylation is predicted by bioinformatics analyses, whereas two-component systems (involving His/Asp phosphorylation) identified in the Euryarchaeota phylum are absent (6–9).

A phosphoproteome study of the thermoacidophilic crenarchaeon *Sulfolobus solfataricus* P2 revealed a vast amount of Ser/Thr/Tyr-phosphorylated proteins (540 detected in total), in almost all arCOGs categories, with an unexpectedly high number of Tyr phosphorylation. A differential phosphorylation pattern was observed in cells grown on glucose *versus* tryptone, and a role of protein phosphorylation in regulating the glycolytic flux in *Sulfolobus* was proposed (10). Further, a phosphoproteome study of the mesophilic euryarchaeon *Halobacterium salinarum* revealed 69 phosphorylated proteins in total (2).

Although a few archaeal protein kinases and phosphatases have been investigated in more detail (7, 11–19), there is still a knowledge gap regarding signal transduction pathways in Archaea and the impact of Ser/Thr/Tyr phosphorylation on cellular processes. Comparative database searches revealed only two protein phosphatases encoded in the genomes of all

From the ‡Molecular Biology of Archaea, Max Planck Institute for terrestrial Microbiology, Karl-von-Frisch Straβe 10, 35043 Marburg, Germany; §Molecular Enzyme Technology and Biochemistry, Biofilm Centre, Faculty of Chemistry, University of Duisburg-Essen, Universitätsstrasse 5, D-45141 Essen, Germany; ¶Institute for Theoretical Chemistry, University of Vienna, Währingerstrasse 17, A-1090 Vienna, Austria; ‖ChELSI Institute, Department of Chemical and Biological Engineering, The University of Sheffield, Mappin Street, Sheffield, S1 3JD, United Kingdom; **Department of Molecular Biosciences, The Wenner-Gren Institute, Stockholm University, Svante Arrhenius väg 20C, SE-106 91, Stockholm, Sweden

⌘ *Author's Choice*—Final version full access.

Received January 10, 2013, and in revised form, September 18, 2013

Published, MCP Papers in Press, September 27, 2013, DOI 10.1074/mcp.M113.027375

[1] The abbreviations used are: PTM, post-translational modification; arCOG, archaeal clusters of orthologous groups; qPCR, quantitative PCR.

members of the *Sulfolobales* order, in comparison to eight predicted protein kinases in *S. solfataricus* alone (7). Similarly, in eukaryotes fewer protein phosphatases are encoded in the genome compared with protein kinases, though the phosphatases of the PPP family often act as multimeric proteins with different catalytic, regulatory and core subunits (20, 21).

Protein phosphatases can be categorized into different families. Ser/Thr-specific PPPs contain a 220 amino acid long catalytic domain that includes motif I (GDXHG), motif II (GDXXDRG), and motif III (GNHE) (22), and Mg^{2+} or Mn^{2+} dependent Ser/Thr phosphatases (PPMs) contain 11 specific motifs (23, 24). Conversely, the phosphotyrosine phosphatase family (PTP) can be subdivided into the PTPs, which are specific for Tyr dephosphorylation, the dual specific PTPs, which can dephosphorylate Ser/Thr and Tyr, and the low molecular weight PTPs. PTP phosphatase family members share a common amino acid motif, CX_5R (20).

Only a few archaeal Ser/Thr- or Tyr-specific protein phosphatases have been characterized. The Ser/Thr phosphatase PP1-arch1 from *S. solfataricus* displays Mn^{2+}-dependent protein phosphatase activity *in vitro* (16). The crystal structure of SsoPTP from *S. solfataricus* has been solved and the specificity toward phosphotyrosine determined *in vitro* (18). Only one additional archaeal PTP has been characterized, the *Tk*-PTP from the euryarchaeon *Thermococcus kodakaraensis* KOD, which exhibits phosphotyrosine as well as phosphoserine, but no phosphothreonine phosphatase activity (17). Finally, the only characterized archaeal member of the PPM family is found in *Thermoplasma volcanium* and has a divalent metal-ion dependent dual-specificity toward phosphorylated Ser/Thr as well as Tyr residues (25).

The creanarcheon *S. acidocaldarius*, which grows optimally at pH 3 and 76 °C, contains two protein phosphatases, the Saci-PTP (phospho Tyr phosphatase), encoded by the *saci0545* gene (*saci_ptp*) and the Saci-PP2A (phospho Ser/Thr phosphatise) encoded by *saci0884* (*saci_pp2a*), which is homologous to the PP2A catalytic subunit of eukaryotic phosphatases. In this study, Saci-PTP and Saci-PP2A were characterized with respect to substrate specificity and kinetic properties. Furthermore, *in vivo* analyses were performed with deletion mutants to investigate the resulting phenotypes, and additional characterization was carried out by RNA-seq and phosphoproteome analysis.

EXPERIMENTAL PROCEDURES

Strains and Growth Conditions—*Escherichia coli* K12 DH5α (Invitrogen, Breda, The Netherlands) and Rosetta (DE3) (Stratagene, La Jolla, CA) were used for cloning and expression studies, respectively. Both strains were grown under standard conditions as reported recently (26).

The markerless in-frame deletion mutants and the uracil auxotrophic parental strain *S. acidocaldarius* MW001 (27) were grown at 76 °C in Brock's basal medium at pH 3.5 (28). The medium was supplemented with 0.1% (w/v) NZ-amine, 0.2% (w/v) sucrose, and 10 μg/ml uracil (water dissolved). The trans-complementation strains of the deletion mutants were grown without uracil because the uracil auxotrophic marker was encoded by the complementation plasmid.

Chemicals—All chemicals were purchased from Sigma-Aldrich (Taufkirchen, Germany), VWR (St. Louis, MO), Carl Roth (Karlsruhe, Germany) or Roche Diagnostics (Mannheim, Germany) in analytical grade. Para-nitrophenylphosphate (pNPP) was purchased from Sigma-Aldrich. The p-Thr-peptide RRA(pT)VA was purchased from Promega (Madison, WI). The p-peptide TEVGKRI(pY)RLVGDKN was synthesized according to the p-peptide of Saci_1938 determined in the phosphoproteome analysis and purchased from PROTEINMODS (Madison, WI). For the characterization of Saci_PTP the p-peptides NIDAIRA(pS)LNIMSR and ETTYERW(pT)TITQRER derived from the respective p-peptides of Saci_1346 and Saci_1857, respectively, determined in the phospho-proteome analysis were purchased from Thermo Fisher Scientific.

Heterologous Expression and Protein Purification—For expression of Saci-PTP (Saci0545) and Saci-PP2A (Saci0884) the genes were amplified by PCR using specific primers (Table I) and cloned into the pET vector system (pET-15b, or pETDuet-1, Novagen). The constructed plasmids were verified by sequencing of both strands (AGOWA, Berlin and MWG Operon, Ebersberg, Germany).

Heterologous expression of Saci-PTP and Saci-PP2A was performed in *E. coli* Rosetta (DE3)-RIL as expression host strain. For purification of the recombinant enzymes, the resulting *E. coli* crude extracts were diluted 1:1 with 50 mM NaH_2PO_4, 300 mM NaCl (pH 8.0, RT), and subjected to a heat precipitation for 20 min at 80 °C. After heat precipitation, the samples were cleared by centrifugation (60,000 $\times$ *g* for 30 min at 4 °C).

For Saci-PP2A and Saci-PTP the supernatant was dialyzed overnight against 50 mM NaH_2PO_4, 300 mM NaCl (pH 8.0, RT), subjected to immobilized metal affinity chromatography (Ni-TED 2000, Macherey-Nagel, pre-equilibrated in 50 mM NaH_2PO_4, 300 mM NaCl (pH 8.0, RT), and eluted in 50 mM NaH_2PO_4, 300 mM NaCl, 250 mM imidiazole (pH 8.0, RT). Fractions containing the recombinant enzymes (analyzed by SDS-PAGE, enzyme activity) were pooled and concentrated via centrifugal concentrators (Vivaspin6, Sartorius Stedim Biotech). From 3.8 g of recombinant cells (wet weight), 1.7 mg Saci-PTP and from 17 g of recombinant cells (wet weight) 0.4 mg Saci-PP2A were obtained.

Saci-PP2A was further purified by ion exchange chromatography and size exclusion chromatography. Briefly, Saci-PP2A was dialyzed overnight against 20 mM Tris/HCl (pH 6.5, 70 °C), subjected to ion exchange chromatography (UNO Q-17; Bio-Rad Laboratories, Hercules, CA) (pre-equilibrated in 20 mM Tris/HCl (pH 6.5, 70 °C)), and eluted with a linear salt gradient from 0 to 1 M NaCl. Afterward, the sample was dialyzed overnight against 50 mM Tris/HCl, 300 mM KCl (pH 6.5, 70 °C) and applied to size exclusion chromatography (HiLoad 26/60 Superdex 200 prep grade; Amersham Biosciences) (pre-equilibrated in 50 mM Tris/HCl, 300 mM KCl (pH 6.5, 70 °C)). The fractions containing the recombinant enzymes were analyzed via Coomassie stained SDS-PAGE and enzyme activity tests, pooled and further used for the enzymatic characterization.

Enzyme Assays—Phosphatase activity was determined in a continuous enzyme assay at 70 °C with pNPP as substrate. For Saci-PTP the standard assay was performed in 0.1 M HEPES/KOH (pH 6.5) with 7 μg protein, whereas for Saci_0884 the assay was performed in 20 mM Tris/HCl, 300 mM KCl (pH 6.5), 5 mM Mn^{2+}, 1 mM EGTA containing 0.25 μg protein in a reaction volume of 300 μl. Enzymatic activity was determined by monitoring the change in absorbance at 403 nm because of the formation of paranitrophenyl (εp-NPP = 18 mM/cm). For each assay three independent measurements were performed.

Protein tyrosine phosphatase activity was determined by using the tyrosine phosphatase assay system (Promega) following the manu-

facturer's instruction. The artificial p-peptides TEVGKRI(pY)RLVGDKN, NIDAIRA(pS)LNIMSR, and ETTYERW(pT)TITQRER were used as substrate. The enzyme activity was determined in a discontinuous enzyme assay at 70 °C in 0.1 M HEPES/KOH (pH 6.5) containing 2 μg Saci-PTP. The phosphate release was measured by using the Serine and Threonine phosphatase malachite-green-based assay system from Promega following the instructions of the manufacturer. For each assay three independent measurements were performed.

Protein serine/threonine phosphatase activity was determined by using the serine/threonine phosphatase assay system (Promega) following the manufacturer's instruction. The artificial p-peptides RRA(pT)VA and TEVGKRI(pY)RLVGDKN were used as substrate. The enzyme activity was determined in a discontinuous enzyme assay at 70 °C in 20 mM Tris/HCl, 300 mM KCl (pH 6.5), 5 mM Mn^{2+}, 1 mM EGTA containing 0.1 μg Saci-PP2A. The phosphate release was measured and visualized by using malachite green. For each assay, three independent measurements were performed.

For enzyme reactions following Michaelis-Menten kinetics the kinetic parameters (V_{max} and K_m) were calculated by iterative curve-fitting using the program Origin 8.6G 64 bit (Microcal Software, Northampton, MA).

Construction of In-frame Deletion Mutants in S. acidocaldarius—Plasmids for deletion mutant construction were cloned using the PCR product of the upstream- and downstream-region of the gene of interest (Primers, supplemental Table S5), overlap PCR was performed to fuse both fragments and the overlap product was ligated with the gene targeting plasmid pSVA406 (27). The constructed plasmids were methylated using *E. coli* ER1821 and transformed into the background strain *S. acidocaldarius* MW001 (uracil auxotrophic strain) as described before (27). The subsequent steps were performed as described by Lassak *et al.* 2012 (29). In short, transformants were first selected on gelrite plates lacking uracil and then counterselected on plates with uracil and 5-FOA. The markerless in-frame deletion mutants of both phosphatase genes (*saci0545* and *saci0884*), designated Δ*saci_ptp* and Δ*saci_pp2a*, respectively, were identified by colony PCR and confirmed by sequencing (MWG Operon, Ebersberg, Germany).

Flow Cytometry Analysis—Aliquots from growing cultures of strains MW001, Δ*saci_ptp* and Δ*saci_pp2ac* were transferred to ice-cold ethanol (final concentration 70% (v/v)). For DNA staining, ~0.5 ml of cell suspension in ethanol was centrifuged at 4 °C for 10 min at 16,000 × *g*. The pellet was resuspended in 1 ml of 10 mM Tris-buffer (pH 7.4) containing 10 mM $MgCl_2$, centrifuged again, and then resuspended in 70 μl of the same buffer. Equal volumes (65 μl) of cell suspension and DNA-specific stain (0.2 mg/ml mithramycin A and 0.04 mg/ml ethidium bromide, also in Tris-$MgCl_2$ buffer) were mixed. The samples were incubated on ice for 30 min before analysis in an Apogee A40 Analyzer flow cytometer equipped with a 405 nm solid-state laser.

Analysis of Cell Size—Microscopy pictures were taken using an Axio Imager.M1 microscope (Zeiss) equipped with a Zeiss Plan Apochromat × 100/1.40 Oil DIC objective and a Cascade:1K CCD camera (Photometrics). Cell size was analyzed automatically with ImageJ and ObjectJ using a modified version of the filaments-91i.ojj project. The results were evaluated with Origin 6.1 (OriginLab Corporation, Northampton, MA, USA).

RNA Isolation and Sample Preparation for RNA-seq Analysis—*S. acidocaldarius* MW001, Δ*saci_ptp,* and Δ*saci_pp2a* were inoculated in triplicate. Cultures were grown to reach an OD_{600} of 0.6 (exponential growth phase) and subsequently samples of the three independent cultures of each strain were pooled in equal amounts to generate one mixed sample per strain. Total RNA samples were isolated from 10 ml of exponentially growing shaking cultures. TRIzol reagent (Invitrogen) was used for total RNA isolation following the instructions of the manufacturer. Residual chromosomal DNA present in RNA samples was removed by RNase-free DNase I (Roche) treatment for 2 h at 37 °C. DNA-free RNA samples were confirmed by PCR amplification using *saci0574* (*sec*Y) primer pairs. Before cDNA synthesis DNA-free RNA samples were fragmented to achieve a molecule size range of 50 to 500 nucleotides. Thus, 6 μg of DNA-free RNA samples were mixed with 4 μl of 5× fragmentation buffer (200 mM Tris acetate, pH 8.2; 500 mM potassium acetate; 150 mM magnesium acetate). The reaction mix was filled up with DEPC H_2O up to 20 μl, incubated at 95 °C for 2.5 min and immediately transferred to ice. The reaction was then cleaned up by using sephadex columns (illustra MicroSpin™ G-25, GE Healthcare). RNA fragmentation range was checked by polyacrylamide gels. Six hundred nanograms of fragmented RNA was used for cDNA synthesis using the SuperScript Double-stranded cDNA Synthesis kit (Invitrogen) and following manufacturer's instructions. The reaction was cleaned by using phenol/chloroform/isoamyl alcohol and cDNA samples were then precipitated by using 3 M NaOAc/100% ethanol and incubated over night at −20 °C. Finally, cDNA samples were washed with 500 μl 70% ethanol. Five nanograms of cDNA were used as starting material for the generation of single-end sequencing libraries with the NEBnext DNA sample preparation kit, as described by manufacturer's protocol. The DNA was ligated to Illumina adaptors, which carried a unique four letter barcode sequence. DNA fragments of 150–500 bp were selected for sequencing. To retain strand specificity the DNA was treated with Uracil DNA-Glycosilase (UDGase) before the PCR amplification. The sequencing was performed by an Illumina Genome Analyzer IIx, multiplexed together with a total of eight samples. The reads were partitioned according to their barcode, stripped from adapter sequences and barcodes and mapped, using default settings, to the *Sulfolobus acidocaldarius* DSM 639 (NC_007181) reference genome, with segemehl (30).

Bioinformatic Analysis of RNA-seq Data—For each protein coding and ncRNA gene, according to the NCBI database, the associated reads were counted. An overview where the reads map to, can be found in supplemental Fig. S8*A*. The overall Illumina sequencing represented 26.6%, 30.2%, 26.5% of genome coverage by the mapped reads for MW001, Δ*saci_ptp* and Δ*saci_pp2a*, respectively. To identify differentially expressed genes among the sample conditions, we used DESeq (version 1.5) (31), which allows estimation of the dispersion within one condition. This estimation is based on the assumption that only a few genes are truly differentially expressed; hence variance across different conditions can be seen as a too conservative estimation of the variance within one condition. From the estimated expected variance and the observed fold change in read counts, the statistical significance of altered RNA abundance can be calculated for every gene. Genes with a p value below 0.054 were considered to be significantly altered in their expression. supplemental Figs. S8*B* and S8*C* shows the correlation among the observed read counts, the fold change in read count among the sample conditions and the significance of the alteration.

RT-qPCR—First Strand cDNA Synthesis Kit (Fermentas) was used for cDNA synthesis according to the manufacturer's instructions. The synthesis was thus performed using random hexamer primers and 1 μg of DNA-free RNA as template. Quantitative PCR (qPCR) analysis was carried out using Maxima SYBR Green/ROX qPCR Master Mix (Fermentas) based on the Sybr green detection system (Real-Time 7300 PCR machine; Applied Biosystems, Foster City, CA). The efficiency of each primer pair was calculated from the average slope of a linear regression curve, which resulted from qPCRs using a 10-fold dilution series (10 pg–10 ng) of *S. acidocaldarius* chromosomal DNA as template. Cq values (quantification cycle) were automatically determined by Real-Time 7300 PCR software (Applied Biosystems) after 40 cycles. Cq values of each transcript of interest were standardized to the Cq value of the reference gene *saci0574* (*secY*) (32). qPCR

reactions with DNA-free RNA samples as template were performed as control. At least three biological replicates of each assessed condition and two technical replicates per qPCR reaction were performed.

Immunoblotting Analysis After Nutrient-limited Growth Conditions—The expression levels of the archaella components FlaB and FlaX were determined as described by Reimann *et al.* 2012 (33). Therefore the background strain *S. acidocaldarius* MW001 and both phosphatase deletion mutants (Δ*saci_ptp* and Δ*saci_pp2a*) were transferred to nutrient-limited medium. The same amount of cells referring to OD_{600} with and without starvation stress treatment were lysed and the proteins separated by SDS-PAGE. The expression levels of FlaB and FlaX were detected by immunoblotting using specific antibodies.

Motility Assay on Semisolid Gelrite Plates—To compare the motility of the background strain *S. acidocaldarius* MW001 to the phosphatase deletion strains (Δ*saci_ptp* and Δ*saci_pp2a*) the two control strains Δ*aapF* (hypermotile strain) and Δ*aapF*Δ*flaH* (nonmotile strain) were used. The strains were spotted on semisolid gelrite plates (0.15% gelrite (w/v)) containing only 0.005% (w/v) tryptone, 0.2% (w/v) dextrin and 10 μg/ml uracil as described before (29, 33). Plates were incubated for 5 days in a humid chamber at 75 °C. Swimming behavior of the different *S. acidocaldarius* strains was analyzed by measuring the swimming radius.

Protein Sample Preparation for Mass Spectrometry Analysis—For phosphoproteome analysis *S. acidocaldarius* MW001, MW010 (Δ*saci_ptp*), and MW025 (Δ*saci_pp2a*) were aerobically grown in a 10 liter fermenter with constant rotational mixing of the cultures. At the OD_{600} 0.8 2 liter samples were taken. The cells were harvested by centrifugation at 9000 × *g* (Beckman Coulter Avanti J-26XP, rotor JLA 8.1) and the pellets immediately frozen in liquid nitrogen.

Cells were washed with cold water and then resuspended in 50 mM phosphate buffer (pH 7.5) and phosphatase inhibitors (5 mM each) comprising 2-glycerol phosphate, sodium fluoride, sodium vanadate, and sodium pyrophosphate (1). Cell extraction was performed using a combination of both ultrasonication and liquid nitrogen (manual grinding with a mortar and pestle). First, cells were sonicated using an ultrasonicator (Branson, Mexico) at a power of 70% for eight times (alternatively 45 s of sonication and 45 s of incubation in ice). Samples were then frozen using liquid nitrogen and ground manually five times. Furthermore, DNase I (100 μg/ml) and N-Octyl- glucoside (a final concentration of 1% (w/v)) were also added to samples to increase solubilization of membrane proteins (1). Samples were then finally sonicated in a water bath containing ice for 10 min before centrifugation at 21,000 × *g* for 20 min at 4 °C. Protein supernatant was collected and quantified using the RC-DC Protein Quantification Assay (Bio-Rad, UK). All chemicals were purchased from Sigma.

A total of 2 mg protein for each sample was denatured in 8 M urea, reduced with 10 mM DTT in 50 mM ammonium bicarbonate at 56 °C for 1 h, then alkylated with 55 mM idoacetamide in 50 mM ammonium bicarbonate at 37 °C for 30 min in the dark. Before trypsin digestion was performed, samples were diluted to a final urea concentration less than 1 M by 40 mM ammonium bicarbonate in 9% acetonitrile (ACN) (34). A trypsin/protein ratio of 1:25 was used for trypsin digestion at 37 °C overnight. Samples were then dried in a vacuum concentrator (Eppendorf, Germany) before resuspension in buffer A consisting of 10 mM KH_2PO_4, 30% acetonitrile, and 0.1% trifluoroacetic acid pH 3.0 for fractionation and cleaning of the sample. Strong cation exchange (SCX) was performed using a HPLC system with UV detector (Dionex, UK) with buffer B used for peptide elution comprising of 10 mM KH_2PO_4, 30% ACN, 0.1% TFA, and 500 mM KCl, pH 3.0 (see (35) for details). Fractions of the sample were then collected every 2 min and peptides were subsequently dried in a vacuum concentrator (Eppendorf, Germany).

Mass Spectrometry Analysis and Data Processing—All dried peptides were then cleaned using a C_{18} Discovery DSC-18 SPE column (Supelco, Sigma) as described elsewhere (36); all fractions were subsequently combined, before analysis on a HCT-Ultra ion trap (Bruker Daltonics, UK) coupled with an Ultimate 3000 nano-flow HPLC (Dionex, UK) consisting of an analytical column (3 mm C_{18}, Dionex-LC Packings) operating at a flow rate of 300 nL/min. Buffer A contained 3% acetonitrile and 0.1% (w/v) formic acid, whereas buffer B contained 97% (w/v) acetonitrile and 0.1% (w/v) formic acid. The 90 min gradient comprised ramping from 3% B to 35% B in the first 70 min, then ramping to 90% B in 5 min, then switching back to 3% of buffer A for 15 min. Peptides eluting from HPLC column were directly submitted to the ion trap.

The PAcIFIC technique was applied for analyzing (combined) cleaned peptides. Details of this technique can be found elsewhere (10, 37). Briefly, resuspended peptides were injected multiple times on the ion trap with collision induced association at each of 10 continuous 1.0 *m/z* intervals across a range of 10 m/z for each LC-MS analysis using a 2.0 *m/z* width and fragmented ions scanned from 100 to 1600 *m/z* with a dynamic ion charge threshold of 160,000. Subsequently, a next (forward) new ten ions was started in the same format as the first run, then this process continued until the considered precursors covered the range from 450 to 1100 *m/z*.

Data from mass spectrometry were then extracted to mgf format using Bruker Data Analysis V4.0 with a MRM script, these were then were searched against the *S. acidocaldarius* database downloaded from NCBI in March 2010 (containing 2223 proteins) using Phenyx V 2.6 (Genebio, Geneva). The searches were performed using parameters as follows: carbamidomethylation of cysteine (fixed modification), oxidation of methionine (variation), and phosphorylation of serine, tyrosine, threonine (variation), trypsin with two missed cleavages. Furthermore, other parameters such as parent, MS/MS, tolerances were set at 2.0 and 0.8 Da, respectively, whereas minimum peptide length, z-score, *p* value and AC score were set at 5, 5.5, 10–15, and 5.5 respectively.

The spectra for all identified phosphopeptides were then automatically processed using *Mathematica* 9.0 (Wolfram Research, Inc.) in order orthogonally to confirm (1) the neutral loss of phosphoric acid (H_3PO_4, mass shift = −98) or metaphosphoric acid (HPO_3, mass shift = −80) from the precursor or/and fragment ions and (2) the presence of at least 5 b or y sequencing ion series. For the automatic annotation, peaks of intensity lower than 10% of the maximal intensity were discarded. The annotated spectra were then manually to ensure the quality of the annotations. Moreover, an independent biological duplicate sample was generated for each strain and an identical analysis carried out. Scores of phosphorylation sites are shown in Table S7. Raw spectra have been submitted to the PRIDE database (http://www.ebi.ac.uk/pride/, with ProteomeXchange accession: PXD000289, and are waiting for an accession number) (38).

RESULTS

Characterization of saci_ptp and saci_pp2a Deletion Mutants—Marker-less gene deletion mutants of the two putative phosphatases, Saci-PTP and Saci-PP2A, were generated using the uracil auxotrophic *S. acidocaldarius* MW001 strain (supplemental Fig. S1). Δ*saci_pp2a* showed slow growth (doubling time 9.5 h) and reached the stationary phase after 130 h, whereas MW001 and Δ*saci_ppt* showed similar growth characteristics (doubling times 5.7 h and 6.3 h, respectively; stationary phase reached after 60 h; supplemental Fig. S2). Notably, the Δ*saci_ptp* cells appeared normal in cell size (1.3 μM ± 0.55 μM), whereas the Δ*saci_pp2a* deletion mutant showed significant size variation (1.46 μM ± 1.08 μM) in com-

parison to MW001 (1.27 μM ± 0.42 μM; supplemental Fig. S3) in microscopy analysis. The larger variation in the cell size distribution of the *saci_pp2a* deletion mutant, as compared with the parental strain and Δ*saci_ptp*, was confirmed by flow cytometry analysis (supplemental Fig. S4*B*). No changes in the DNA content distributions, reflecting the relative lengths of the cell cycle periods (39), could be detected in either deletion mutant, as compared with the parental strain (supplemental Fig. S4*A*), indicating no major effects on cell cycle regulation or progression through the different cell cycle phases. The aberrant phenotype of the Δ*saci_pp2a* mutant could be partially restored in a trans-complementation experiment, resulting in a growth curve and cell shape distribution similar to those of the parental strain (supplemental Figs. S5*A* and S5*B*).

TABLE I
Kinetic properties of protein phosphatases in S. acidocaldarius at 70 °C

Substrate	Saci-PTP		Saci-PP2A	
	K_m (μM)	V_{max} (U/mg)	K_m (μM)	V_{max} (U/mg)
pNPP	530	3.7	2500	4.3
TEVGKRI(pY)RLVGDKN	530	9.2	No activity	No activity
RRA(pT)VA	-	-	53.6	192.6
NIDAIRA(pS)LNIMSR	423	0.3	-	-
ETTYERW(pT)TITQRER	490	0.07	-	-

Enzymatic Characterization of Saci-PTP and Saci-PP2A—Saci-PTP and Saci-PP2A were heterologously expressed (supplemental Fig. S6) in *E. coli*, purified, and analyzed *in*

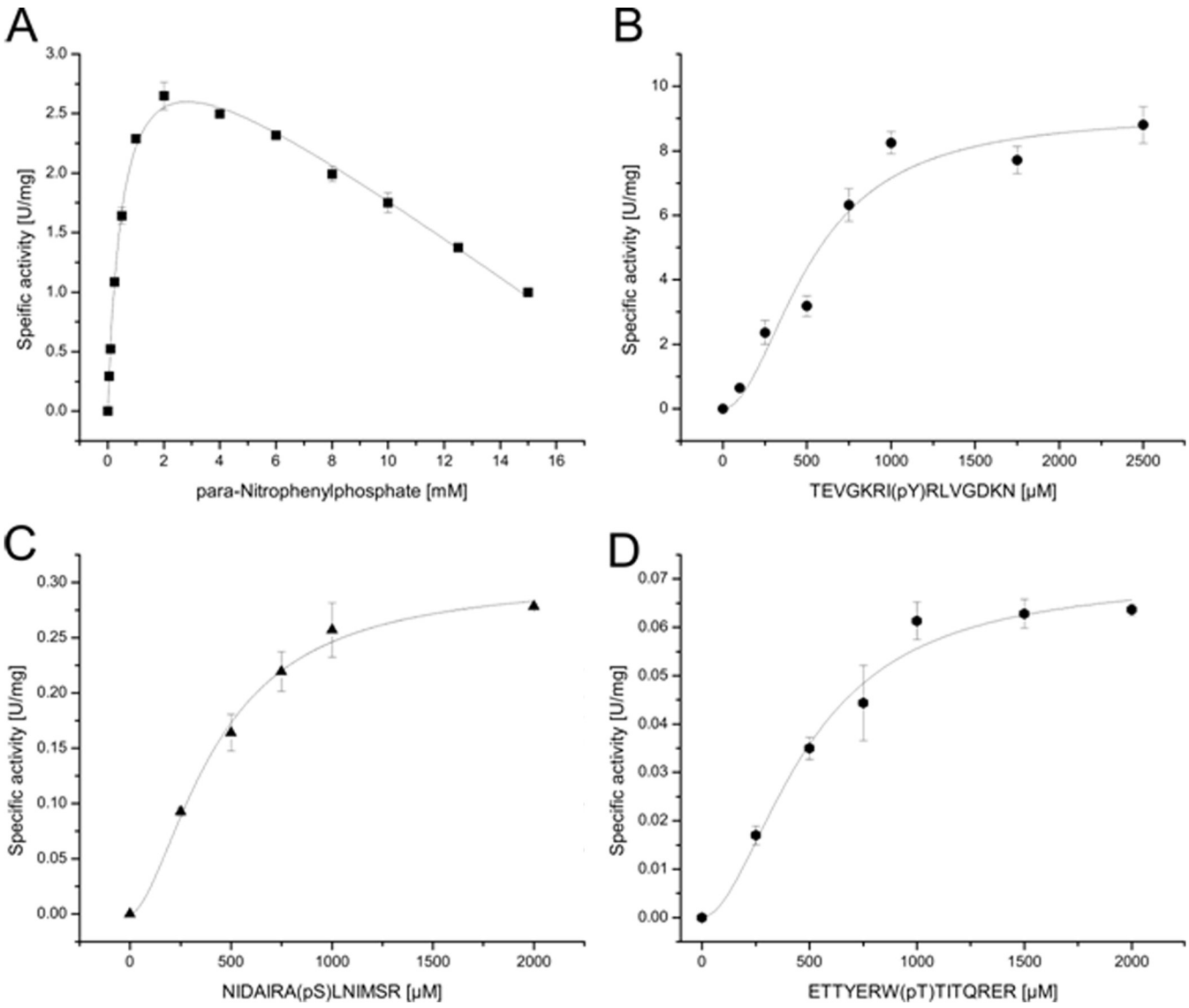

FIG. 1. **Biochemical characterization of the protein phosphatases Saci-PTP.** The activity of Saci-PTP was analyzed in the presence of pNPP (*A*), of the phospho-Tyr peptide TEVGKRI($_{p}$Y)RLV (*B*), the phospho-Ser peptide NIDAIRA($_{p}$S)LNIMSR (*C*), and the phospho-Thr peptide ETTYERW-($_{p}$T)TITQRER (*D*). All experiments were performed at 70 °C in triplicate. Saci_PTP showed general phosphatase activity with pNPP as substrate (*A*). Furthermore, Saci-PTP displayed a dual-specific phosphatase activity using p-Tyr peptides (*B*) as well as p-Ser (*C*) and p-Thr (*D*) peptides as substrate.

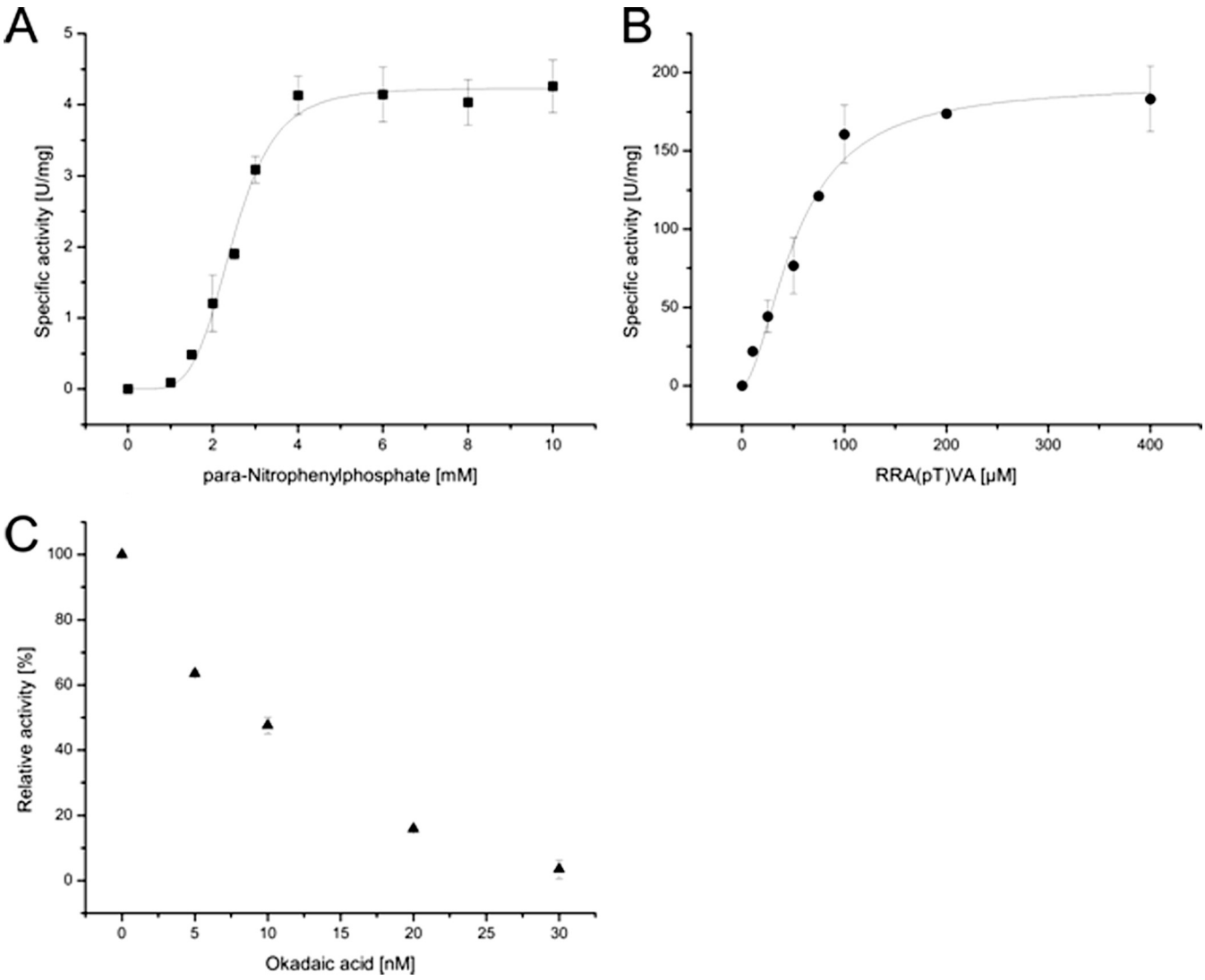

FIG. 2. **Biochemical characterization of the protein phosphatases Saci-PP2A.** The activity of Saci-PP2A was determined in the presence of pNPP (*A*), the phospho-Thr peptide RRA(pT)VA (*B*) as well as in the presence of okadaic acid (p-Thr peptide RRA(pT)VA)(*C*). All experiments were performed at 70 °C in triplicate. Saci_PP2A revealed phosphatase activity with pNPP as well as the p-Thr peptide, whereas no activity was observed with the p-Tyr peptide. Furthermore, Saci_PP2A was significantly inhibited in presence of okadaic acid, a typical inhibitor of PPPs.

vitro. Both enzymes showed similar phosphatase activity with the pNPP substrate at 70 °C (Table I). For Saci-PTP substrate inhibition was observed at pNPP concentrations above 2 mM (k_{irr}-value of 0.17 (U/mg)mM^{-1}) (Fig. 1*A*). For Saci-PP2A cooperativity was observed at pNPP concentrations below 2 mM (Hill coefficient of 4.9) (Fig. 2*A*).

The substrate specificity of Saci-PTP was addressed with the p-Tyr peptide TEVGKRI(pY)RLVGDKN as substrate (Table I). In addition, low activities were observed with the p-Thr peptide ETTYERW(pT)TITQRER and the p-Ser peptide ETTYERW(pT)TITQRER, indicating dual protein phosphatase specificity (Table I; Fig. 1). However, the maximal velocity (V_{max}-value) for the p-Tyr peptide was 30- and 131-fold higher as compared with the p-Ser and the p-Thr peptide, respectively (Table I). The affinity (K_m value) toward all three phospho-peptides was similar (Table I), indicating that p-Tyr was the preferred substrate.

Phosphatase activity was only observed with the p-Thr peptide RRA(pT)VA for Saci-PP2A (Table I; Fig. 2). In addition, the analysis revealed that Saci-PP2A requires divalent metal ions for activity. The highest activity was observed with Cu^{2+}, followed by Mn^{2+}, Ni^{2+}, Mg^{2+}, Cd^{2+} and Co^{2+}, in the presence of EGTA (supplemental Fig. S7). When EGTA was replaced by EDTA, no PP2A activity could be observed. In the absence of divalent metal ions the enzyme was inactive. Activity tests in the presence of okadaic acid, an inhibitor of PPPs, revealed a strong inhibitory effect (56% activity in presence of 10 nM okadaic acid; Fig. 2*C*).

Whole-transcriptome Profiling of Δsaci_ptp and Δsaci_pp2a by RNA-seq—Three cDNA libraries were constructed and we

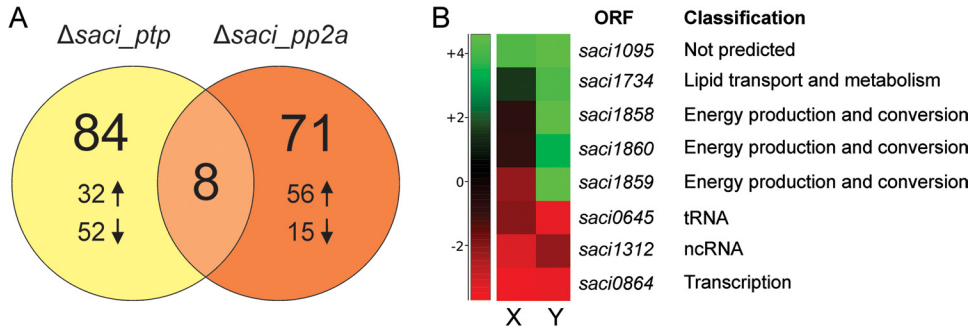

FIG. 3. **Transcriptionally regulated genes in Δ*saci_ptp* and Δ*saci_pp2a* as compared with the strain MW001.** *A*, The number of differentially regulated gene products in Δ*saci_ptp* and Δ*saci_pp2a* are depicted in a Venn diagram. Up and down arrows represent the number of genes which were found to be either up- or down-regulated for each deletion strain. In Δ*saci_ptp*, most genes were down-regulated, whereas in Δ*saci_pp2a* most were up-regulated. Eight genes were differentially regulated in both phosphatase deletion strains. *B*, Heat-map representation of all eight commonly regulated genes in Δ*saci_ptp* (X) and Δ*saci_pp2a* (Y). The graph is based on the differential gene expression analysis by RNA-seq, showing all genes that are significantly altered in their expression in both deletion strains. The right side panel shows the functional classification for each gene product.

obtained 1,835,618, 1,472,609, and 1,560,420 qualified Illumina read pairs for MW001, Δ*saci_ptp* and Δ*saci_pp2a*, respectively. An average of 82.6% of the reads were mapped to rRNA and tRNA sequences, whereas 14.5% mapped to protein-coding sequences (CDS) and 2.8% to intergenic regions in the *S. acidocaldarius* genome (supplemental Fig. S8).

A differential gene expression analysis was performed for each mutant strain, as compared with the MW001 parent strain. The transcript levels of 84 and 71 genes were significantly (threshold of twofold change) altered in Δ*saci_ptp* and Δ*saci_pp2a,* respectively (Fig. 3*A* and Fig. 4; supplemental Table S3*A* and S3*B*). Although the majority of the changes corresponded to down-regulated genes in Δ*saci_ptp* (52 of 84 genes), the opposite was observed in Δ*saci_pp2a* (56 of 71 genes up-regulated; Fig. 3*A* and Fig. 4). To functionally categorize the regulated genes, an arCOG category analysis was performed (40, 41). A majority of the differentially affected transcripts encoded proteins belonging to the categories unknown function (arCOG S), energy production and conversion (arCOG C), and transcription (arCOG K) (supplemental Table S4).

Only eight common genes were significantly affected in both deletion strains (Fig. 3*B*). Five of these were affected in the same direction (either up- or down-regulated), whereas three were divergently expressed (down-regulated in Δ*saci_ptp* whereas up-regulated in Δ*saci_pp2a*; Fig. 3*B* and Fig. 4). These three, *saci1858*, *saci1859*, and *saci1860*, corresponded to genes encoding SoxNL complex components (complex III of the respiratory chain; *saci1858* and *saci1859* encode mono-heme cytochrome b558–566 (CbsA and CbsB), whereas *saci1860* encodes a Riske Fe-S protein (SoxL)) (42). The two downstream genes of the *soxNL* complex operon, *saci1861* (*soxN*) and *saci1862* (*odsN*), were also up-regulated in Δ*saci_pp2a* (Fig. 4). Moreover, Δ*saci_pp2a* displayed augmented transcript levels of components of one of the three terminal oxidases (complex IV; the DoxBCE complex (*saci0098* and *saci0099*); (Fig. 4). Four additional genes belonging to the energy metabolism and conversion arCOG category were up-regulated in Δ*saci_pp2a*, encoding a cytochrome/quinol oxidase (Saci0097), a polyferredoxin (Saci1802), a thioredoxin (Saci1823), and the sulfocyanine SoxE-like protein (Saci2096) (Fig. 4).

Increased transcript levels of three transcriptional regulators (Saci1171, Saci1180, and Saci2193) were detected in Δ*saci_pp2a*. Interestingly, *saci1180* and *saci1171* are located up- and downstream of the archaellum operon (formerly archaeal flagellum (43)) (Fig. 4) and have been shown to activate archaella gene expression (44). Three additional genes of the archaellum operon, encoding FlaI, FlaG, and FlaX (*saci1173*, *saci1176*, and *saci1177*), were found to be up-regulated in Δ*saci_pp2a* cells, in agreement with a regulatory role for protein phosphorylation in archaella expression (33).

In contrast to Δ*saci_pp2a*, the Δ*saci_ptp* strain showed a predominant down-regulation of gene expression, including genes encoding components of the SoxABCD oxidase complex (*saci2088* (*soxB*) and *saci2086* (*soxD*)) (Fig. 4) (45). Additionally, transcript levels of ORFs encoding a thioredoxin-like (Saci0359) protein, a Rieske-like protein (Saci1963) and an isocitrate-lyase (Saci2191) were down-regulated. To illustrate the transcription changes, a model of the *S. acidocaldarius* branched respiratory electron transport chain is depicted in Fig. 5 with the transcriptional response of each phosphatase mutant on the oxidase complexes indicated. Among the few up-regulated genes in Δ*saci_ptp*, three predicted transcriptional regulators were among the highest expressed genes (*saci0065*, *saci0455*, and *saci1787*). The target genes for these regulators are, unknown.

To confirm the RNA-seq data the expression of all archaellum operon genes, together with selected respiratory chain genes, was analyzed by quantitative RT-PCR. Whereas no significant changes in expression levels could be observed in the Δ*saci_ptp* deletion strain, all seven genes of the archaellum operon were found to be up-regulated in the Δ*saci_pp2a* cells (Fig. 6), confirming the result of the analysis (Fig. 4). The

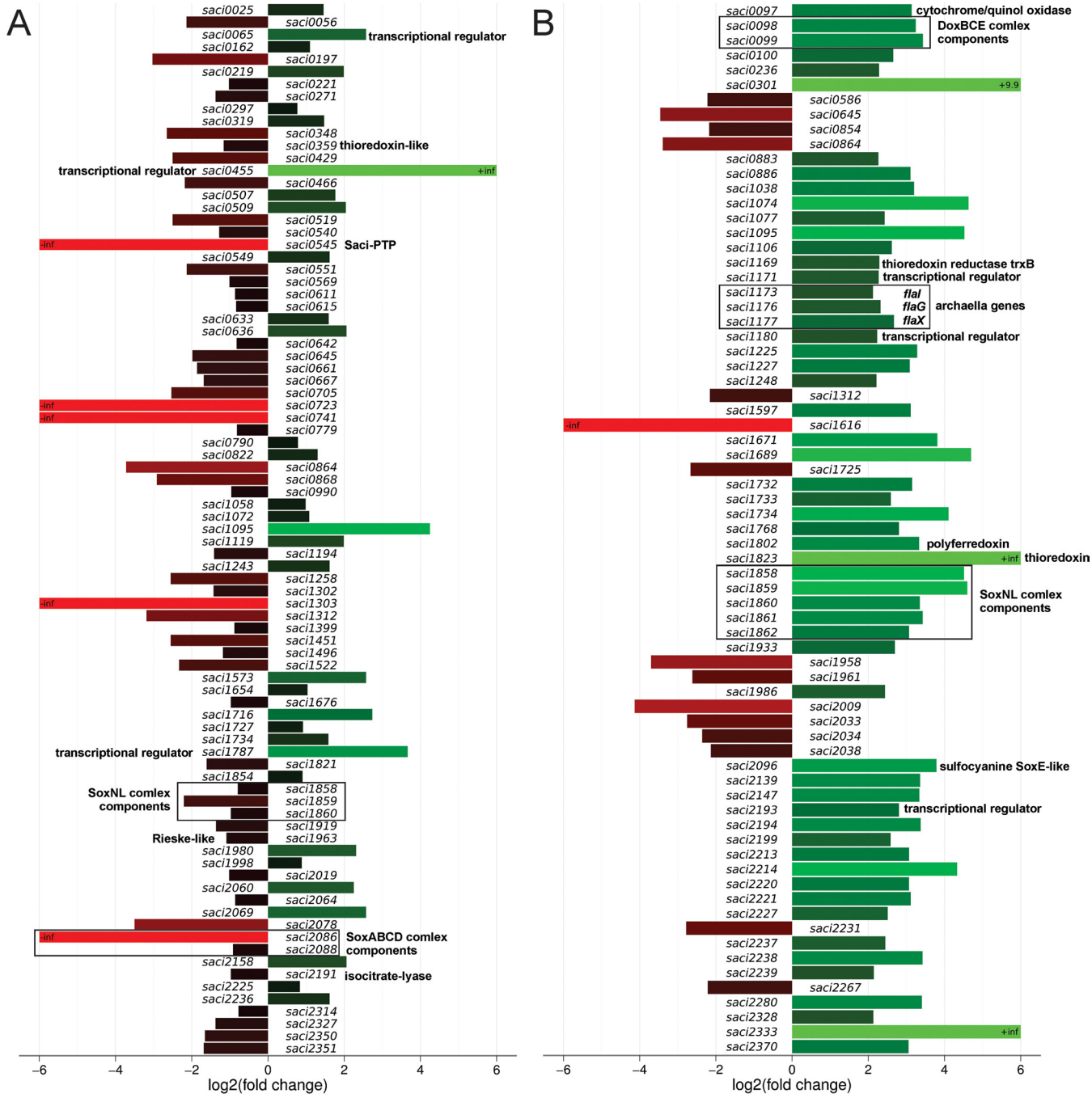

FIG. 4. **Bar plot representation of the transcriptomic changes in Δ*saci_ptp* and Δ*saci_pp2a*.** A differential gene expression analysis was performed for each deletion strain, Δ*saci_ptp* (*A*) and Δ*saci_pp2a* (*B*), in comparison to the wild-type strain MW001. All genes of whose expression was significantly altered (≥twofold) are shown. Red and green bars represent down- and up-regulated genes, respectively. Genes with a *p* value below 0.054 were considered to be significantly differentially regulated. The annotation of selected genes is indicated to the right of each column.

induction of the genes encoding SoxNL complex components and the SoxABCDL terminal oxidase in Δ*saci_pp2a* was also confirmed (Fig. 6).

Phosphoproteomic Analysis of MW001, Δsaci_ptp and Δsaci_pp2a—Phosphoproteomic analyses (including cytoplasmic and membrane proteins) were performed on the three strains (MW001, Δ*saci_pp2a* and Δ*saci_ptp*) in late exponential growth phase ($OD_{600\ nm}$ of 0.8), as described previously for *S. solfataricus* P2 (10). Two biological replicates were analyzed for each strain and a false discovery rate (FDR) for each experiment was also estimated. As a result, averaged FDRs of 3.4%, 3.0%, and 3.6% were estimated for MW001,

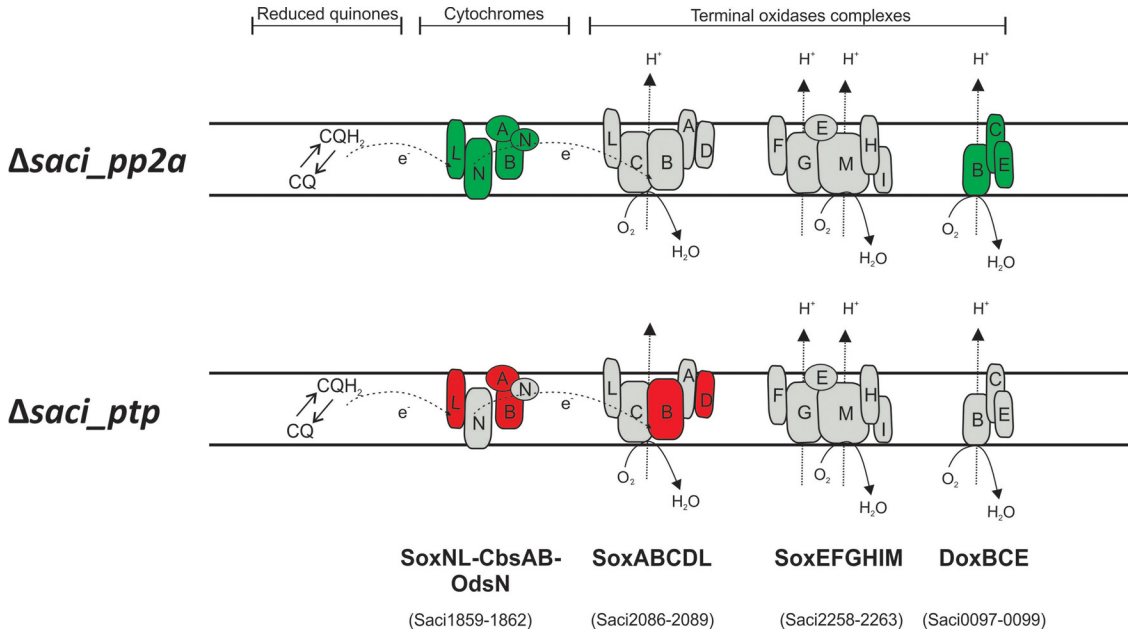

FIG. 5. **Proposed model of *S. acidocaldarius* branched aerobic respiratory chain.** The respiratory chain model is based on separate biochemical characterization studies. Electrons from NADH or succinate oxidation presumably enter electron transport chain via NADH: quinone oxidoreductases or succinate:quinone oxidoreductases (not shown). Reduced quinones (CQH_2) then deliver electrons to cytochrome oxidase bc1 complex SoxLN-CbsAB-OdsN (42) and subsequently to one of the three terminal oxidase complexes. These terminal complexes are SoxABCD-SoxL (45, 54, 55), the bb3 terminal oxidase complex SoxEFGHIM (56–58), and the DoxBCE (59). Components whose transcript levels were altered in each deletion strain are depicted either in red or green for down- and up-regulation, respectively. Gene identifiers for each component are shown below.

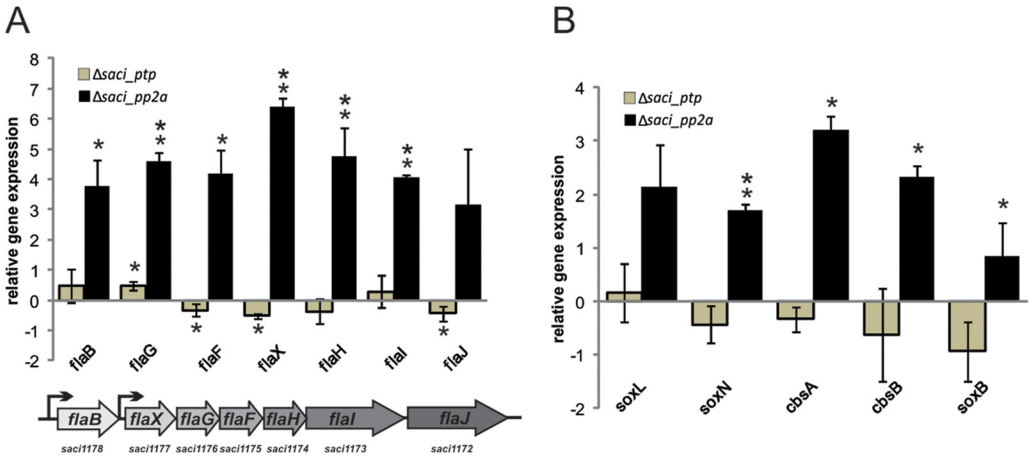

FIG. 6. **Differential expression levels of archaella operon genes and respiratory chain genes in Δ*saci_pp2a* and Δ*saci_ptp*.** Total RNA isolated from *S. acidocaldarius* MW001, Δ*saci_pp2a* and Δ*saci_ptp* cultures were used for cDNAs synthesis. qRT-PCR analysis was performed using specific primers for each archaella component (*A*) and components of the terminal oxidase complexes (*B*). Relative transcript levels of each gene were normalized to an internal control gene *secY*. The values reflect the fold change compared with cDNA prepared from MW001. The means and standard deviations of three biological replicates are shown. Up-regulation of all archaella and the terminal oxidase genes in the *saci_pp2a* deletion strain reflect the RNA-seq results. * significant (p value ≤ 0.05), ** highly significant (p value ≤ 0.01).

Δ*saci_ptp*, and Δ*saci_pp2a* strains, respectively. Overall, 1206 phosphorylated peptides (p-peptides) from 801 unique phosphorylated proteins (phosphoproteins) were identified, with an overall pS/pT/pY %-ratio of 35.6/28.1/36.2. In MW001, 54 phosphopeptides from 54 phosphoproteins (pS/pT/pY %-ratio of 32.9/21.3/45.7) were detected, in Δ*saci_pp2a* 477 phosphopeptides from 387 phosphoproteins (35.0/27.2/37.7), and in Δ*saci_ptp* 715 phosphopeptides from 551 phosphoproteins (36.4/29.1/34.5) (supplemental Table S1, Table II). The identified phosphoproteins were categorized according to arCOG functional code (40, 41). Unique phosphoproteins were identified in 21 out of 26 arCOG functional categories (supplemental Table S2), indicating an important role of phosphorylation in most cellular processes.

TABLE II
Comparison of different phosphoproteome studies

Organism	Genome size (Mb)	Strain	P-proteins (no.)	P-peptides (no.)	P-sites (no.)	pSer (%)	pThr (%)	pTyr (%)
S. acidocaldarius Total	2.2		801	1246	1855	35.6	28.1	36.2
S. acidocaldarius		MW001	54	54	77	31.2	23.4	45.5
		Δ*saci_pp2a*	387	477	734	35.0	27.2	37.7
		Δ*saci_ptp*	551	715	1044	36.4	29.1	34.5
S. solfataricus Total (40)	2.9	P2	540	690	1318	25.8	20.6	53.6
S. solfataricus (40)	2.9	P2	311^{Glu}	343^{Glu}	580^{Glu}	25.2^{Glu}	18.5^{Glu}	55.3^{Glu}
			311^{Tryp}	384^{Tryp}	810^{Tryp}	25.1^{Tryp}	21.5^{Tryp}	53.4^{Tryp}
Halobacterium salinarum (2)	2.7	R1	69	90	81	86	12	1
Lactococcus lactis (60)	2.4	Il1403	63	102	73	46.5	50.6	2.7
Bacillus subtilis (1)	4.2	168	78	103	78	69.2	20.5	10.3
Escherichia coli K12(61)	4.6	K12-MG1655	79	105	81	67.9	23.5	8.6
Zea mays leaf (62)	2.065	B73	125	149	157	89.8	9.6	0.6
Synechococcus sp. (63)	3.4	PCC 7002	245	280	410	43.9	42.44	13.66
Pseudomonas putida(51)	5.9	PNL-MK25	40	56	53	52.8	39.6	7.5
Pseudomonas aeruginosa (51)	6.3	PAO1	23	57	55	52.7	32.7	14.5
Campylobacter jejuni (64)	1.6	NCTC11168	36	58	35	-	-	-
Streptococcus pneumonia (65)	2.1	D39	84	102	163	47.2	43.8	9
Streptomyces coelicolor (66)	9.1	A3 (2)	40	44	44	34.1	52.3	13.6
Streptomyces coelicolor (67)	9.1	M145	127	260	289	46.8	48	5.2
Klebsiella pneumonia (68)	5.5	NTUH-K2044	81	117	93	31.2	15.1	25.8
Mycoplasma pneumoniae (69)	0.8	M129	63	16	16	53.3	46.7	0
Helibacter pylori (70)	1.7	26695	67	80	126	42.8	38.7	18.5
Mycobacterium tuberculosis (71)	4.4	H37Rv	301	381	516	60	40	0
Listeria monocytogenes (72)	2.9	EGDe	112	155	143	65	30.1	4.9
Clostridium acetobutyicum (73)	4.1	ATCC824	61	82	107	42	47.7	10.3
Plasmodium falciparum (74)	23.3	3D7	919	2418	2541	84.4	13.2	2.4
Trichomonas vaginalis (75)	176.4	ATCC30236	82	93	103	71.8	21.4	6.8
Thermus thermophilus (76)	2.1	HB8	48	52	50	64	26	10
Rhodopseudomonas palustris (77)	5.5	CGA010	54^{CH}	100^{CH}	60^{CH}	63.3^{CH}	16.1^{CH}	19.4^{CH}
			42^{PH}	74^{PH}	56^{PH}	58.9^{PH}	23.2^{PH}	17.9^{PH}
Trypanosoma cruzi (78)	67	DM28c	753	-	2572	84.1	14.9	1.0
Toxoplasma gondii (79)	80	RH	2793^{i}	$11,822^{i}$	$12,793^{i}$	87.2	12.6	0.25
			3506^{p}	$21,498^{p}$	$24,298^{p}$	89.3	10.5	0.25
Plasmodium falciparum (79)	23	3D7	1673	7835	8463	89.1	10.4	0.51
Arabidopsis thaliana (80)	119.7	-	598	962	609	86	14	0.16

Target Proteins for Phosphorylation—The phosphoproteome data set was specifically screened for proteins belonging to the aerobic respiration chain and the archaellum (Table III). Six proteins of the arCOG family C (energy production and conversion) were found to be phosphorylated, including SoxC (Saci2087) and SoxI (Saci2258), which belong to different terminal oxidase complexes (Fig. 5). Furthermore, three von Willebrand domain-containing proteins (Saci0977, Saci1209, and Saci1211) involved in archaellum synthesis were phosphorylated at different residues. One of these, ArnB (Saci1211), has previously been shown to be involved in negative regulation of the archaellum *in vivo* (33). Also the membrane-associated FlaJ protein (Saci1172), involved in archaella assembly, contained four phosphorylation sites and was identified in both phosphatase deletion mutants. The predicted positive transcriptional regulator ArnR1 (Saci1171)(44) located directly adjacent to the archaellum operon was also phosphorylated. Seventeen additional predicted transcriptional regulators also contained phosphorylation sites, demonstrating the importance of this PTM in transcriptional regulation in Archaea. Five predicted serine/threonine kinases were also identified as phosphorylated in the deletion strains.

Regulation of Cell Motility Via Reversible Protein Phosphorylation—The up-regulation of the seven archaella genes in Δ*saci_pp2a* (Figs. 4 and 6), was investigated at the protein phosphorylation level. The parental strain and both deletion strains were cultivated in rich medium and then transferred to medium without supplemented nutrients for 5 h, a treatment that has been shown to induce archaella biosynthesis (29). Samples before and after induction were analyzed by immunoblotting with specific antibodies against the archaellin protein FlaB and the accessory protein FlaX. Both proteins were induced by nutrient limitation stress in the parent strain MW001, and to the same extent in Δ*saci_ptp*. In contrast, Δ*saci_pp2a* showed a FlaB signal already before induction, and highly increased levels of FlaB and FlaX after nutrient limitation as compared with MW001 and Δ*saci_ptp* (Fig. 7*A*).

TABLE III
Phosphoproteins related to aerobic respiration, motility, transcriptional regulation and phosphorylation identified in the S. acidocaldarius phosphoproteome

Protein	arCOG category	Functional arCOG annotation	Strain
Saci2087	C	Cytochrome b subunit of the bc complex (SoxC)	Δ*saci_ptp*
Saci2250	C	Pyruvate:ferredoxin oxidoreductase or related 2-oxoacid:ferredoxin oxidoreductase, gamma subunit	Δ*saci_ptp*
Saci2258	C	Predicted subunit of heme/copper-type cytochrome/quinol oxidase (SoxI)	Δ*saci_ptp*
Saci2263	C	Heme/copper-type cytochrome/quinol oxidase, subunit 1 and 3	Δ*saci_pp2a*
Saci2273	C	Fe-S oxidoreductase	Δ*saci_pp2a*
Saci2316	C	Fe-S oxidoreductase	Δ*saci_pp2a* Δ*saci_ptp*
Saci0977	R	Uncharacterized protein containing a von Willebrand factor type A (vWA) domain	MW001 Δ*saci_ptp*
Saci1209	R	Uncharacterized protein containing a von Willebrand factor type A (vWA) domain	Δ*saci_ptp*
Saci1211	R	Protein containing a von Willebrand factor type A (vWA) domain ArnB	Δ*saci_ptp*
Saci1172	NU	Archaeal flagella assembly protein J	Δ*saci_ptp* Δ*saci_pp2a*
Saci1171	K	Predicted transcriptional regulator	Δ*saci_ptp*
Saci0446	K	Transcriptional regulator, contains HTH domain	Δ*saci_ptp*
Saci0501	K	Predicted transcriptional regulator, PadR family	Δ*saci_pp2a*
Saci0882	K	Predicted transcriptional regulator	Δ*saci_pp2a*
Saci1068	K	Transcriptional regulator, MarR family	Δ*saci_ptp*
Saci1161	K	Sugar-specific transcriptional regulator TrmB	Δ*saci_ptp*
Saci1242	K	Transcriptional regulator, contains HTH domain	Δ*saci_pp2a*
Saci1344	K	Predicted transcriptional regulator	MW001 Δ*saci_ptp*
Saci1502	K	Predicted transcriptional regulator, contains C-terminal CBS domains	Δ*saci_ptp*
Saci1523	K	Predicted transcriptional regulator, contains ATP-binding and HTH domains	Δ*saci_ptp* Δ*saci_pp2a*
Saci1528	K	Predicted transcriptional regulator, contains ATP-binding and HTH domains	Δ*saci_pp2a*
Saci1588	K	Transcriptional regulator (IclR family)	Δ*saci_ptp*
Saci1658	K	Transcriptional regulator (Lrp/AsnC family)	Δ*saci_ptp*
Saci2116	K	Predicted transcriptional regulator, c-terminal HTH-like domain	Δ*saci_pp2a*
Saci2352	K	Predicted transcriptional regulator, PadR family	Δ*saci_ptp*
Saci0635	K	Transcriptional regulator, xre family	Δ*saci_ptp*
Saci1505	K	Transcriptional regulator, xre family	Δ*saci_ptp*
Saci2005	K	Predicted transcriptional regulator	Δ*saci_pp2a*
Saci0965	TD	Serine/threonine protein kinase involved in cell cycle control	Δ*saci_pp2a*
Saci1193	RTKL	Membrane associated serine/threonine protein kinase	Δ*saci_pp2a* Δ*saci_ptp*
Saci1694	RTKL	Membrane associated serine/threonine protein kinase	Δ*saci_pp2a* Δ*saci_ptp*
Saci1869	RTKL	Membrane associated serine/threonine protein kinase	Δ*saci_ptp*
Saci1875	RTKL	Membrane associated serine/threonine protein kinase	Δ*saci_pp2a*

The swimming ability of the wild-type strain and both deletion mutants was investigated using a motility assay. MW001, Δ*saci_ptp*, Δ*saci_pp2a*, a hypermotile positive control (Δ*aapF*) and a nonmotile negative control (Δ*aapF*Δ*flaH*) were spotted on semi-solid Gelrite-plates containing low amounts of nutrients (29, 46). After 5 days of incubation at 76 °C, MW001 and Δ*saci_ptp* showed only slight motility. In contrast, the motility of Δ*saci_pp2a* was comparable to the hypermotile Δ*aapF*, which lacks the Aap pili (Archaeal adhesive pili) (Fig. 7*B*), indicating a major impact of protein phosphorylation on cell motility in *S. acidocaldarius*.

DISCUSSION

We report a detailed characterization of two protein phosphatases of *S. acidocaldarius*, Saci-PTP and Saci-PP2A. Saci-PTP displayed dual-specific Ser/Thr and Tyr phosphatase activity, whereas Saci-PP2A was specific for Ser/Thr dephosphorylation. Differences in phosphorylation and gene expression patterns were observed in deletion strains, suggesting roles for both phosphatases in signal transduction pathways. The changes observed when the gene encoding Saci-PP2A was deleted were similar to responses observed when *S. acidocaldarius* cultures experience severe nutrient limitation. Up-regulation of archaellar and respiratory chain components may enable the organism to evade unfavorable conditions by promoting archaellar assembly and providing energy for archaella-driven motility.

Comparison of the phosphoproteome of *S. acidocaldarius* with that of *S. solfataricus* (40) revealed an overlap of 94 proteins, although the different experimental approaches (deletion mutants compared with growth on different carbon sources) should be taken into account. Conserved phosphorylation sites were identified in 13 of the 94 overlapping proteins. A single conserved site was identified in ten of these, whereas two sites were detected in Saci0940, Saci0381, and Saci2134. None of the 15 sites had a score higher than 0.5

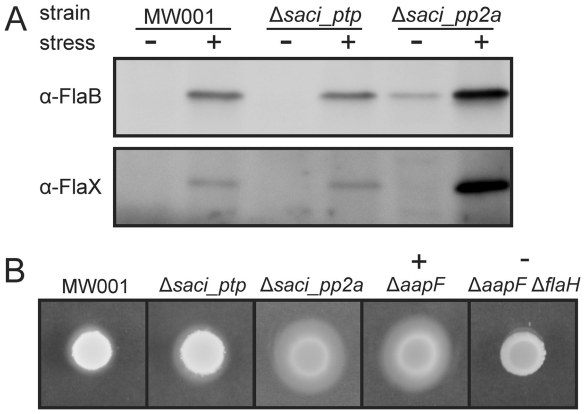

FIG. 7. **Impact of phosphatase deletion on archaella expression and motility.** *A*, For the nutrient limitation assay MW001, Δ*saci_ptp* and Δ*saci_pp2a* were grown to an OD_{600} of about 0.4 in Brock medium supplemented with 0.1% NZ-amine, 0.2% sucrose and 10 μg/ml uracil and then transferred to medium lacking the nutrient source. After 6 h samples were collected and immunoblotting was performed with specific antibodies against the archaellum proteins FlaB and FlaX. The amount of protein in Δ*saci_ptp* is comparable to the strain MW001, whereas for Δ*saci_pp2a* highly elevated expression of FlaB and FlaX was observed after the starvation stress. Interestingly, already before stress induction the FlaB levels were increased in the Saci-PP2A deletion mutant. *B*, The wild type strain MW001, the two phosphatase deletion strains Δ*saci_ptp* and Δ*saci_pp2a*, the hypermotile positive control strain Δ*aapF* and the negative nonmotile strain Δ*aapF*Δ*flaH* were spotted on semi-solid Gelrite dishes and incubated for 5 days at 76 °C. Only a small halo is visible for MW001 and Δ*saci_ptp*, whereas Δ*saci_pp2a* was as hypermotile as the positive control strain.

(required to score as a phosphorylation site) in searches using DISPHOS 1.3 software. The highest scores were obtained for the conserved pThr sites in Saci1549 (V-type ATP synthase subunit B; score 0.477) and Saci1715 (dihydroxyacid dehydratase; score 0.263). Although the 15 phosphorylation sites only represent a small fraction of all identified sites and therefore may not provide sufficient data, difficulties in prediction of archaeal phosphorylation sites were also reported in a phosphoproteome study of *H. salinarium*, using the Motif X tool (2).

The number of identified phosphorylation targets in *S. acidocaldarius* is high, with 801 phosphoproteins identified in the three strains. Only for *Plasmodium falciparum* (1673) and *Toxoplasma gondii* (intracellular samples 2793; purified samples 3506) have higher numbers been recorded. However, both are eukaryotes and possess several-fold larger proteomes as compared with *S. acidocaldarius*. Also, the number of identified phosphoproteins in the *S. acidocaldarius* parent strain MW001 alone was low (54), and similar to the number observed in the euryarchaeon *H. salinarum* (69).

Deletion of the phosphatases increased the number of phosphoproteins, as expected. When comparing the Δ*saci_pp2a* strain with the MW001 parent, the number of phosphorylation sites increased from 77 to 734, whereas the pSer/pThr/pTyr %-ratio remained similar. In the Δ*saci_ptp* strain the phosphorylation sites increased even more, from 77 to 1044, and the pSer/pThr/pTyr %-ratio was also influenced by the deletion (31.2/23.4/45.5 compared with 36.4/29.1/34.5). In Δ*saci_pp2a* the dephosphorylation of pSer and pThr is prevented, which should result in a higher amount of pSer and pThr, whereas in Δ*saci_ptp* strain the amount of pTyr should also be increased. A similar discrepancy was reported for *H. salinarum*, in which a Δ*serB* strain was compared with the corresponding wild type. The gene *serB* encodes the only phosphoserine phosphatase annotated in the genome of *H. salinarium* and the deletion increased the number of phosphoproteins from 26 (wild type) up to 62 (Δ*serB* strain). In addition, the amount of pSer was increased in a similar way from 25 (wild type) up to 64 (Δ*serB* strain). However, the amount of pThr as well as pTyr was also increased from 5 (wild type) to 10 (Δ*serB* strain) and 0 (wild type) to 1 (Δ*serB* strain). Usually, one would expect that the deletion of SerB only affects the number of phosphoproteins and the amount of pSer and that the amount of pThr and pTyr should be the same. Nonetheless, the enzymatic properties of SerB were not investigated until now, the data imply that the protein is not specific for pSer.

Bioinformatic analysis revealed that SerB shares no similarity with Saci-PTP or Saci-PP2A. For *S. acidocaldarius*, the unexpected change of the pSer/pThr/pTyr %-ratio could partly be explained by the biochemical properties of Saci-PTP and Saci-PP2a, as the Saci-PTP displays dual activity. It is also possible that deletion of the protein phosphatases induces other PTMs to compensate for the loss of regulation.

The high amount of Tyr phosphorylation in both *Sulfolobus* species appears to be a crenarchaeal feature, rather than a thermoadaptation property or a general archaeal feature. The phosphoproteome of the hyperthermophilic bacterium *Thermus thermophilus* was recently analyzed, revealing 48 phosphoproteins with 50 phosphorylation sites and a pSer/pThr/pTyr %-ratio of 64/26/10. The amount of pTyr is in accordance with amounts identified in other prokaryotic phosphoproteome studies (Table II), supporting the conclusion that Tyr phosphorylation is a crenarchaeal feature rather than a thermoadaptation. Both *T. thermophilus* and *H. salinarum* contain two-component phosphorylation systems, which are absent in crenarchaea. It is thus possible that that the extensive Tyr phosphorylation in *Sulfolobus* species provides a means to compensate for the absence of two-component systems in these organisms.

The expression of several transcription factors was highly affected in the deletion mutants. However, in the absence of information about target genes, the physiological consequences remain unknown. In contrast, an explanation can be provided for the effects of deletion of Saci-PP2A on archaellum and respiration chain genes. In *S. acidocaldarius* two regulatory systems have been shown to be involved in control of archaella biosynthesis, the ArnA (Saci1210) and ArnB (Saci1211) repressors of the *flaX-flaJ* gene cluster (33), and the ArnR (Saci1180) and ArnR1 (Saci1171) positive regulators

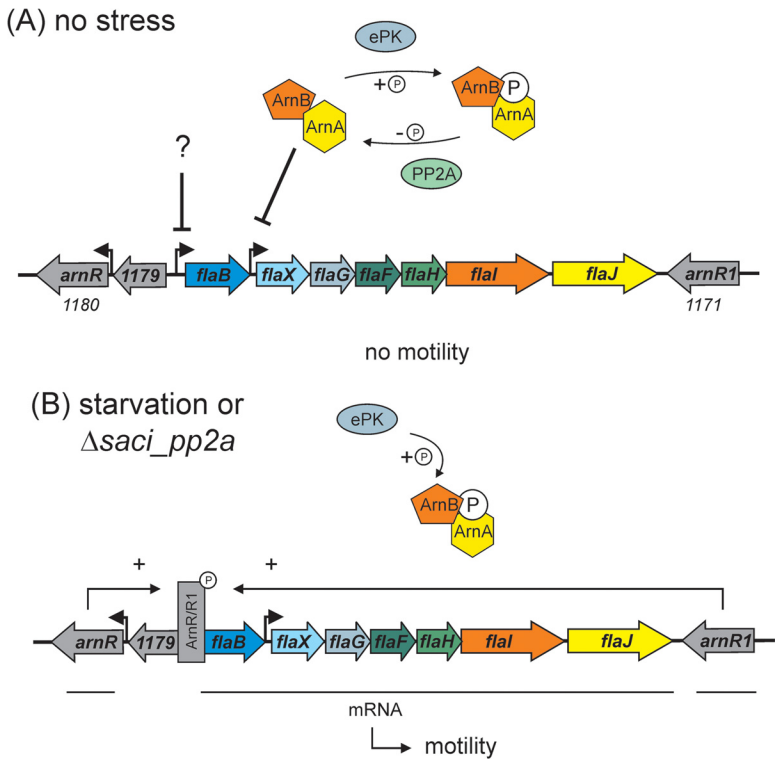

FIG. 8. **Model of the involvement of phosphorylation in the regulation of motility in *S. acidocaldarius*.** During exponential growth (*A*) archaellum synthesis from the *flaB-flaJ* (*saci1178–1172*) operon is repressed. Part of the repression network are ArnA (Saci1210) and ArnB (Saci1211) that are phosphorylated and dephosphorylated by ePK (Saci1193) and PP2A, respectively. ArnA and B closely interact and repress the *flaX* promoter (35). Probably another, yet unknown, factor is repressing the *flaB* promoter. When S. *acidocaldarius* cells enter stationary phase and undergo starvation, or in the Δ*saci_pp2a* deletion mutant (*B*), the ArnaA/B complex exists only in its phosphorylated form and repression is released. Moreover, the expression of ArnR (Saci1180) and ArnR1 (Saci1171) is induced and these factors then drive high expression of FlaB which leads to the assembly of archaella on the cell surface and therefore to increased motility.

of *flaB* expression (See model in Fig. 8) (44). ArnR1 and ArnR, were up-regulated in the Δ*saci_pp2a* strain and, in addition, ArnR1 was found to be phosphorylated in the Δ*saci_ptp* strain. Further, in the biochemical characterization, ArnA and ArnB were phosphorylated by the Saci1193 kinase and dephosphorylated by the Saci-PP2A phosphatase (for a model see Fig. 8) (33). In the phosphoproteome data, this kinase and ArnB revealed *in vivo* phosphorylation in the kinase domain and the C-terminal region, respectively, (see supplemental Table S1). In addition, the *saci1193* gene displays strong cell-cycle-specific induction of transcription (47), with >16-fold up-regulation around the cell division stage, just before a two- to fourfold up-regulation of the archaellum-encoding genes (*flab - flaJ*; *saci1174 - saci1178*), further linking these functions together. In *S. tokodaii*, ArnA has been shown to bind to the FlaX promoter (48). However, no effect on transcription of FlaB and FlaX was observed in the *S. acidocaldarius arnA* deletion strain, suggesting that regulation instead may occur via protein-protein interaction (33). The C-terminal phosphorylation sites of ArnB shown here could thus affect docking of ArnA (33). Under nutrient starvation conditions archaella biosynthesis is highly induced and expression levels are comparable to those in the Δ*saci_pp2a* strain, therefore both conditions lead to a situation, at least regarding to archaella expression, where the negative regulators (ArnA/B) are inactive because of permanent phosphorylation and the positive regulators (ArnR/R1) can enhance archaella expression (see Fig. 8).

Thioredoxin (Saci1823), thioredoxin reductase (Saci1169) and peroxiredoxin (Saci2227) encoding genes were up-regulated in the Δ*saci_pp2a* strain. These were also up-regulated in a study on on oxidative stress in *S. solfataricus*, but no archaealla gene up-regulation was found (49). In all three domains of life, these proteins are involved in disulfide bond shuffling during oxidative stress conditions. The thioredoxin reductase gene is located immediately adjacent to the archaella genes and the ArnR1 regulator and the protein was, in addition, found to be phosphorylated. Hence, nutrient limitation leads both to archaella expression and to oxidative stress responses to avoid cellular damage. In summary, the ArnA/ArnB and ArnR/R1 regulatory systems of archaella expression constitute the first complex regulatory network involving protein phosphorylation to be investigated in crenarchaea.

Surface structure-driven motility is an energy-consuming process and archaella assembly therefore has to be tightly controlled. Several genes involved in energy conversion, including those encoding the SoxNL, SoxABCDL, and DoxBCE respiratory chain complexes, were differentially regulated in the phosphatase deletion strains as compared with the parental strain (Fig. 4). Recently, an association of the flagellar switch-motor complex to the NADH-ubiquinone oxidoreductase and the F_0F_1 ATP synthase was demonstrated in the bacterium *Escherichia coli*, and predicted to function as a local energy supply for flagellar movement (50). The up-regulation of archaella genes in *S. acidocaldarius* may similarly be connected to the up-regulation of genes involved in the res-

piratory chain. Possible interactions of energy generating complexes with the archaella basal body should therefore be investigated. Phosphorylation of respiratory chain components has also been reported in phosphoproteomic studies of *Pseudomonas* spp (51)., *Saccharomyces cerevisiae* mitochondria (52), human muscle mitochondria (53) and *S. solfataricus* (10).

This study provides the first insights into the *in vitro* and *in vivo* functions of the two *S. acidocaldarius* protein phosphatases, Saci-PTP and Saci-PP2A. The RNA-seq and phosphoproteomics studies of the deletion mutants shed light on the multitude of cellular processes affected by reversible protein phosphorylation. In particular, we demonstrate that SaciPP2A is involved in the complex signal transduction pathway regulating the expression of the *S. acidocaldarius* archaellum, and also plays a major role in the control of aerobic respiration and oxidative stress responses.

* JR was supported by a DFG grant (AL 1206/4-1) and SVA and AO were supported by intramural funds of the Max Planck Society. DE was supported by DFG grant (SI 642/10-1). FA was supported by GEN-AU project "regulatory ncRNAs". PCW and TKP were supported by the EPSRC (EP/E036252/1 and EP/I031812/1). RB and ACL were supported by Swedish Research Council grant 621-2010-5551.

[S] This article contains supplemental Figs S1 to S9 and Tables S1 to S7.

‡‡ To whom correspondence should be addressed: Molecular Biology of Archaea, Max Planck Institute for Terrestrial Microbiology, Karl-von-Frisch Straβe 10, 35043 Marburg, Germany. Tel.: +49 6421178426; E-mail: albers@mpi-marburg.mpg.de.

§§ These authors contributed equally.

REFERENCES

1. Macek, B., Mijakovic, I., Olsen, J. V., Gnad, F., Kumar, C., Jensen, P. R., and Mann, M. (2007) The serine/threonine/tyrosine phosphoproteome of the model bacterium Bacillus subtilis. *Mol. Cell. Proteomics* **6,** 697–707
2. Aivaliotis, M., Macek, B., Gnad, F., Reichelt, P., Mann, M., and Oesterhelt, D. (2009) Ser/Thr/Tyr protein phosphorylation in the archaeon *Halobacterium salinarum*–a representative of the third domain of life. *PloS One* **4,** e4777
3. Pawson, T., and Scott, J. D. (2005) Protein phosphorylation in signaling - 50 years and counting. *Trends Biochem. Sci.* **30,** 286–290
4. Johnson, L. N., and Lewis, R. J. (2001) Structural basis for control by phosphorylation. *Chem. Rev.* **101,** 2209–2242
5. Westheimer, F. H. (1987) Why nature chose phosphates. *Science* **235,** 1173–1178
6. Galperin, M. Y. (2005) A census of membrane-bound and intracellular signal transduction proteins in bacteria: bacterial IQ, extroverts and introverts. *BMC Microbiol.* **5,** 35
7. Kennelly, P. J. J. (2003) Archaeal protein kinases and protein phosphatases: insights from genomics and biochemistry. *Biochem. J.* **370,** 373–389
8. Kim, D., and Forst, S. (2001) Genomic analysis of the histidine kinase family in bacteria and archaea. *Microbiology* **147,** 1197–1212
9. Koretke, K. K., Lupas, A. N., Warren, P. V., Rosenberg, M., and Brown, J. R. (2000) Evolution of two-component signal transduction. *Mol. Biol. Evolution* **17,** 1956–1970
10. Esser, D., Pham, K. T., Reimann, J., Albers, S. V., Siebers, B., and Wright, P. C. (2012) Change of carbon source causes dramatic effects in the phospho-proteome of the Archaeon *Sulfolobus solfataricus*. *J. Proteome Res.* **11,** 4823–4833
11. Lower, B. H., Bischoff, K. M., and Kennelly, P. J. (2000) The archaeon *Sulfolobus solfataricus* contains a membrane-associated protein kinase activity that preferentially phosphorylates threonine residues in vitro. *J. Bacteriol.* **182,** 3452–3459
12. Lower, B. H., and Kennelly, P. J. (2003) Open reading frame sso2387 from the Archaeon *Sulfolobus solfataricus* encodes a polypeptide with protein-serine kinase activity. *J. Bacteriol.* **185,** 3436–3445
13. Lower, B. H., Potters, M. B., and Kennelly, P. J. (2004) A phosphoprotein from the archaeon *Sulfolobus solfataricus* with protein-serine/threonine kinase activity. *J. Bacteriol.* **186**, 463–472
14. Wang, B., Yang, S., Zhang, L., and He, Z. G. (2010) Archaeal eukaryote-like serine/threonine protein kinase interacts with and phosphorylates a forkhead-associated-domain-containing protein. *J. Bacteriol.* **192,** 1956–1964
15. Oxenrider, K. A., and Kennelly, P. J. (1993) A protein-serine phosphatase from the halophilic Archaeon. Haloferax volcanii. *Biochem. Biophys. Res. Commun.* **194,** 1330–1335
16. Leng, J., Cameron, A. J., Buckel, S., and Kennelly, P. J. (1995) Isolation and cloning of a protein-serine/threonine phosphatase from an archaeon. *J. Bacteriol.* **177,** 6510–6517
17. Jeon, S.-J., Fujiwara, S., Takagi, M., Tanaka, T., and Imanaka, T. (2002) Tk-PTP, protein tyrosine/serine phosphatase from hyperthermophilic archaeon *Thermococcus kodakaraensis* KOD1: enzymatic characteristics and identification of its substrate proteins. *Biochem. Biophys. Res. Commun.* **295,** 508–514
18. Chu, H. M., and Wang, A. H. (2007) Enzyme-substrate interactions revealed by the crystal structures of the archaeal Sulfolobus PTP-fold phosphatase and its phosphopeptide complexes. *Proteins* **66,** 996–1003
19. Solow, B., Young, J. C., and Kennelly, P. J. (1997) Gene cloning and expression and characterization of a toxin-sensitive protein phosphatase from the methanogenic archaeon *Methanosarcina thermophila* TM-1. *J. Bacteriol.* **179,** 5072–5075
20. Shi, L., Potts, M., and Kennelly, P. J. (1998) The serine, threonine, and/or tyrosine-specific protein kinases and protein phosphatases of prokaryotic organisms: a family portrait. *FEMS Microbiol. Rev.* **22,** 229–253
21. Hubbard, M. J., and Cohen, P. (1993) On target with a new mechanism for the regulation of protein phosphorylation. *Trends Biochem. Sci.* **18,** 172–177
22. Barton, G. J., Cohen, P. T., and Barford, D. (1994) Conservation analysis and structure prediction of the protein serine/threonine phosphatases. Sequence similarity with diadenosine tetraphosphatase from *Escherichia coli* suggests homology to the protein phosphatases. *Eur. J. Biochem.* **220,** 225–237
23. Bork, P., Brown, N. P., Hegyi, H., and Schultz, J. (1996) The protein phosphatase 2C (PP2C) superfamily: detection of bacterial homologues. *Protein Sci.* **5,** 1421–1425
24. Barford, D. (1996) Molecular mechanisms of the protein serine/threonine phosphatases. *Trends Biochem. Sci.* **21,** 407–412
25. Dahche, H., Abdullah, A., Ben Potters, M., and Kennelly, P. J. (2009) A PPM-family protein phosphatase from the thermoacidophile *Thermoplasma volcanium* hydrolyzes protein-bound phosphotyrosine. *Extremophiles* **13,** 371–377
26. Zaparty, M., Esser, D., Gertig, S., Haferkamp, P., Kouril, T., Manica, A., Pham, T. K., Reimann, J., Schreiber, K., Sierocinski, P., Teichmann, D., van, Wolferen, M., von, Jan, M., Wieloch, P., Albers, S. V., Driessen, A. J., Klenk, H. P., Schleper, C., Schomburg, D., van, der, Oost, J., Wright, P. C., Siebers, B. (2010) "Hot standards" for the thermoacidophilic archaeon *Sulfolobus solfataricus*. *Extremophiles* **14,** 119–142
27. Wagner, M., van Wolferen, M., Wagner, A., Lassak, K., Meyer, B. H., Reimann, J., and Albers, S. V. (2012) Versatile genetic tool box for the Crenarchaeote *Sulfolobus acidocaldarius*. *Frontiers Microbiol.* **3,** 214
28. Brock, T. D., Brock, K. M., Belly, R. T., and Weiss, R. L. (1972) Sulfolobus: a new genus of sulfur-oxidizing bacteria living at low pH and high temperature. *Arch. Mikrobiol.* **84,** 54–68
29. Lassak, K., Neiner, T., Ghosh, A., Klingl, A., Wirth, R., and Albers, S. V. (2012) Molecular analysis of the crenarchaeal flagellum. *Mol. Microbiol.* **83,** 110–124
30. Hoffmann, S., Otto, C., Kurtz, S., Sharma, C. M., Khaitovich, P., Vogel, J., Stadler, P. F., and Hackermüller, J. (2009) Fast mapping of short sequences with mismatches, insertions and deletions using index structures. *PLoS Computat. Biol.* **5,** 10
31. Anders, S., and Huber, W. (2010) Differential expression analysis for sequence count data. *Genome Biol.* **11,** R106
32. Van der Sluis, E. O., Nouwen, N., Koch, J., De Keyzer, J., Van der Does, C., Tampé, R., and Driessen, A. J. (2006) Identification of two interaction

sites in SecY that are important for the functional interaction with SecA. *J. Mol. Biol.* **361,** 839–849
33. Reimann, J., Lassak, K., Khadouma, S., Ettema, T. J., Yang, N., Driessen, A. J., Klingl, A., and Albers, S. V. (2012) Regulation of archaella expression by the FHA and von Willebrand domain-containing proteins ArnA and ArnB in Sulfolobus acidocaldarius. *Mol. Microbiol.* **86**, 24–36
34. Gan, C. S., Reardon, K. F., and Wright, P. C. (2005) Comparison of protein and peptide prefractionation methods for the shotgun proteomic analysis of *Synechocystis* sp. PCC 6803. *Proteomics* **5,** 2468–2478
35. Zaparty, M., Esser, D., Gertig, S., Haferkamp, P., Kouril, T., Manica, A., Pham, T. K., Reimann, J., Schreiber, K., Sierocinski, P., Teichmann, D., Van Wolferen, M., Von Jan, M., Wieloch, P., Albers, S. V., Driessen, A. J. M., Klenk, H.-P., Schleper, C., Schomburg, D., Van der Oost, J., Wright, P. C., and Siebers, B. (2010) "Hot standards" for the thermoacidophilic archaeon *Sulfolobus solfataricus. Extremophiles* **14,** 119–142
36. Chong, P. K., and Wright, P. C. (2005) Identification and characterization of the *Sulfolobus solfataricus* P2 proteome. *J. Proteome Res.* **4,** 1789–1798
37. Panchaud, A., Scherl, A., Shaffer, S. A., Haller, P. D. Von, Kulasekara, H. D., Miller, S. I., and Goodlett, D. R. (2009) Precursor acquisition independent from ion count : how to dive deeper into the proteomics ocean. *Anal. Chem.* **81,** 6481–6488
38. Vizcaíno, J. A., Côté, R. G., Csordas, A., Dianes, J. A, Fabregat, A., Foster, J. M., Griss, J., Alpi, E., Birim, M., Contell, J., O'Kelly, G., Schoenegger, A., Ovelleiro, D., Pérez-Riverol, Y., Reisinger, F., Ríos, D., Wang, R., and Hermjakob, H. (2013) The PRoteomics IDEntifications (PRIDE) database and associated tools: status in 2013. *Nucleic Acids Res.* **41,** D1063–D1069
39. Bernander, R., and Poplawski, A. (1997) Cell cycle characteristics of thermophilic archaea. *J. Bacteriol.* **179,** 4963–4969
40. Esser, D., Kouril, T., Zaparty, M., Sierocinski, P., Chan, P. P., Lowe, T., Van der Oost, J., Albers, S.-V., Schomburg, D., Makarova, K. S., and Siebers, B. (2011) Functional curation of the *Sulfolobus solfataricus* P2 and *S. acidocaldarius* 98–3 complete genome sequences. *Extremophiles* **15,** 711–712
41. Makarova, K. S., Sorokin, A. V., Novichkov, P. S., Wolf, Y. I., and Koonin, E. V. (2007) Clusters of orthologous genes for 41 archaeal genomes and implications for evolutionary genomics of archaea. *Biol. Direct* **2**, 33
42. Hiller, A., Henninger, T., Schäfer, G., and Schmidt, C. L. (2003) New genes encoding subunits of a cytochrome bc1-analogous complex in the respiratory chain of the hyperthermoacidophilic crenarchaeon *Sulfolobus acidocaldarius. J. Bioenergetics Biomembranes* **35,** 121–131
43. Jarrell, K. F., and Albers, S.-V. (2012) The archaellum: an old motility structure with a new name. *Trends Microbiol.* **20,** 307–312
44. Lassak, K., Peeters, E., Wróbel, S., and Albers, S. V. (2013) The one-component system ArnR: a membrane-bound activator of the crenarchaeal archaellum. *Mol. Microbiol.* **88,** 125–139
45. Lübben, M., Warne, A., Albracht, S. P., and Saraste, M. (1994) The purified SoxABCD quinol oxidase complex of *Sulfolobus acidocaldarius* contains a novel haem. *Mol. Microbiol.* **13,** 327–335
46. Henche, A. L., Koerdt, A., Ghosh, A., and Albers, S. V. (2012) Influence of cell surface structures on crenarchaeal biofilm formation using a thermostable green fluorescent protein. *Environmental Microbiol.* **14,** 779–793
47. Lundgren, M., and Bernander, R. (2007) Genome-wide transcription map of an archaeal cell cycle. *Proc. Natl. Acad. Sci. U.S.A.* **104,** 2939–2944
48. Duan, X., and He, Z. G. (2011) Characterization of the specific interaction between archaeal FHA domain-containing protein and the promoter of a flagellar-like gene-cluster and its regulation by phosphorylation. *Biochem. Biophys. Res. Commun.* **407,** 242–247
49. Maaty, W. S., Wiedenheft, B., Tarlykov, P., Schaff, N., Heinemann, J., Robison-Cox, J., Valenzuela, J., Dougherty, A., Blum, P., Lawrence, C. M., Douglas, T., Young, M. J., and Bothner, B. (2009) Something old, something new, something borrowed; how the thermoacidophilic archaeon *Sulfolobus solfataricus* responds to oxidative stress. *PloS One* **4,** e6964
50. Zarbiv, G., Li, H., Wolf, A., Cecchini, G., Caplan, S. R., Sourjik, V., and Eisenbach, M. (2012) Energy complexes are apparently associated with the switch-motor complex of bacterial flagella. *J. Mol. Biol.* **416,** 192–207
51. Ravichandran, A., Sugiyama, N., Tomita, M., Swarup, S., and Ishihama, Y. (2009) Ser/Thr/Tyr phosphoproteome analysis of pathogenic and non-pathogenic *Pseudomonas* species. *Proteomics* **9,** 2764–2775
52. Ohlmeier, S., Hiltunen, J. K., and Bergmann, U. (2010) Protein phosphorylation in mitochondria–a study on fermentative and respiratory growth of *Saccharomyces cerevisiae. Electrophoresis* **31,** 2869–2881
53. Zhao, X., León, I. R., Bak, S., Mogensen, M., Wrzesinski, K., Højlund, K., and Jensen, O. N. (2011) Phosphoproteome analysis of functional mitochondria isolated from resting human muscle reveals extensive phosphorylation of inner membrane protein complexes and enzymes. *Mol. Cell. Proteomics* **10**, M110.000299
54. Gleissner, M., Kaiser, U., Antonopoulos, E., and Schafer, G. (1997) The archaeal SoxABCD complex is a proton pump in *Sulfolobus acidocaldarius*. *J. Biol. Chem.* **272,** 8417–8426
55. Lübben, M., Kolmerer, B., and Saraste, M. (1992) An archaebacterial terminal oxidase combines core structures of two mitochondrial respiratory complexes. *EMBO J.* **11,** 805–812
56. Castresana, J., Lübben, M., and Saraste, M. (1995) New archaebacterial genes coding for redox proteins: implications for the evolution of aerobic metabolism. *J. Mol. Biol.* **250,** 202–210
57. Komorowski, L., Verheyen, W., and Schäfer, G. (2002) The archaeal respiratory supercomplex SoxM from *S. acidocaldarius* combines features of quinole and cytochrome c oxidases. *Biol. Chem.* **383,** 1791–1799
58. Lübben, M., Arnaud, S., Castresana, J., Warne, a, Albracht, S. P., and Saraste, M. (1994) A second terminal oxidase in *Sulfolobus acidocaldarius. Eur. J. Biochem.* **224,** 151–159
59. Purschke, W. G., Schmidt, C. L., Petersen, A., and Schäfer, G. (1997) The terminal quinol oxidase of the hyperthermophilic archaeon *Acidianus ambivalens* exhibits a novel subunit structure and gene organization. *J. Bacteriol.* **179,** 1344–1353
60. Soufi, B., Gnad, F., Jensen, P. R., Petranovic, D., Mann, M., Mijakovic, I., and Macek, B. (2008) The Ser/Thr/Tyr phosphoproteome of *Lactococcus lactis* IL1403 reveals multiply phosphorylated proteins. *Proteomics* **8,** 3486–3493
61. Macek, B., Gnad, F., Soufi, B., Kumar, C., Olsen, J. V., Mijakovic, I., and Mann, M. (2008) Phosphoproteome analysis of *E. coli* reveals evolutionary conservation of bacterial Ser/Thr/Tyr phosphorylation. *Mol. Cell. Proteomics : MCP* **7,** 299–307
62. Bi, Y. D., Wang, H. X., Lu, T. C., Li, X. H., Shen, Z., Chen, Y. B., and Wang, B. C. (2011) Large-scale analysis of phosphorylated proteins in maize leaf. *Planta* **233,** 383–392
63. Yang, M., Qiao, Z., Zhang, W., Xiong, Q., Zhang, J., Li, T., Ge, F., and Zhao, J. (2013) Global phosphoproteomic analysis reveals diverse functions of serine/threonine/tyrosine phosphorylation in the model Cyanobacterium *Synechococcus* sp. strain PCC 7002. *J. Proteome Res.* **12,** 1909–1923
64. Voisin, S., Watson, D. C., Tessier, L., Ding, W., Foote, S., Bhatia, S., Kelly, J. F., and Young, N. M. (2007) The cytoplasmic phosphoproteome of the Gram-negative bacterium *Campylobacter jejuni*: Evidence for modification by unidentified protein kinases. *Proteomics* **7,** 4338–4348
65. Sun, X., Ge, F., Xiao, C. L., Yin, X. F., Ge, R., Zhang, L. H., and He, Q. Y. (2009) Phosphoproteomic analysis reveals the multiple roles of phosphorylation in pathogenic bacterium *Streptococcus pneumoniae. J.Proteome Res.* **9,** 275–282
66. Parker, J. L., Jones, A. M., Serazetdinova, L., Saalbach, G., Bibb, M. J., and Naldrett, M. J. (2010) Analysis of the phosphoproteome of the multicellular bacterium *Streptomyces coelicolor* A3 (2) by protein/peptide fractionation, phosphopeptide enrichment and high-accuracy mass spectrometry. *Proteomics* **10,** 2486–2497
67. Manteca, A., Ye, J., Sanchez, J., and Jensen, O. N. (2011) Phosphoproteome analysis of *Streptomyces* development reveals extensive protein phosphorylation accompanying bacterial differentiation. *J. Proteome Res.* **10,** 5481–5492
68. Lin, M. H., Hsu, T. L., Lin, S. Y., Pan, Y. J., Jan, J. T., Wang, J. T., Khoo, K. H., and Wu, S. H. (2009) Phosphoproteomics of *Klebsiella pneumoniae* NTUH-K2044 reveals a tight link between tyrosine phosphorylation and virulence. *Mol. Cell. Proteomics* **8,** 2613–2623
69. Schmidl, S. R., Gronau, K., Pietack, N., Hecker, M., Becher, D., and Stülke, J. (2010) The phosphoproteome of the minimal bacterium *Mycoplasma pneumoniae* analysis of the complete known ser/thr kinome suggests the existence of novel kinases. *Mol. Cell. Proteomics* **9,** 1228–1242
70. Ge, R., Sun, X., Xiao, C., Yin, X., Shan, W., Chen, Z., and He, Q. Y. (2011) Phosphoproteome analysis of the pathogenic bacterium *Helicobacter pylori* reveals over representation of tyrosine phosphorylation and multiply phosphorylated proteins. *Proteomics* **11,** 1449–1461

71. Prisic, S., Dankwa, S., Schwartz, D., Chou, M. F., Locasale, J. W., Kang, C. M., Bemis, G., Church, G. M., Steen, H., and Husson, R. N. (2010) Extensive phosphorylation with overlapping specificity by *Mycobacterium tuberculosis* serine/threonine protein kinases. *Proc. Natl. Acad. Sci. U. S. A.* **107,** 7521–7526
72. Misra, S. K., Milohanic, E., Aké, F., Mijakovic, I., Deutscher, J., Monnet, V., and Henry, C. (2011) Analysis of the serine/threonine/tyrosine phosphoproteome of the pathogenic bacterium *Listeria monocytogenes* reveals phosphorylated proteins related to virulence. *Proteomics* **11,** 4155–4165
73. Bai, X., and Ji, Z. (2012) Phosphoproteomic investigation of a solvent producing bacterium *Clostridium acetobutylicum. Appl. Microbiol. Biotechnol.* **1–11**
74. Lasonder, E., Green, J. L., Camarda, G., Talabani, H., Holder, A. A., Langsley, G., and Alano, P. (2012) The *Plasmodium falciparum* schizont phosphoproteome reveals extensive phosphatidylinositol and cAMP-protein kinase A signaling. *J. Proteome Res.* **11,** 5323–5337
75. Yeh, Y. M., Huang, K. Y., Richie Gan, R. C., Huang, H. D., Wang, T. C. V., and Tang, P. (2013) Phosphoproteome profiling of the sexually transmitted pathogen *Trichomonas vaginalis. J. Microbiol. Immunol. Infect.* **46,** 366–373
76. Takahata, Y., Inoue, M., Kim, K., Iio, Y., Miyamoto, M., Masui, R., Ishihama, Y., and Kuramitsu, S. (2012) Close proximity of phosphorylation sites to ligand in the phosphoproteome of the extreme thermophile *Thermus thermophilus* HB8. *Proteomics* **12,** 1414–1430
77. Hu, C. W., Lin, M. H., Huang, H. C., Ku, W. C., Yi, T. H., Tsai, C. F., Chen, Y. J., Sugiyama, N., Ishihama, Y., Juan, H. F., and Wu, S. H. (2012) Phosphoproteomic analysis of *Rhodopseudomonas palustris* reveals the role of pyruvate phosphate dikinase phosphorylation in lipid production. *J. Proteome Res.* **11,** 5362–5375
78. Marchini, F. K., De Godoy, L. M., Rampazzo, R. C., Pavoni, D. P., Probst, C. M., Gnad, F., Mann, M., and Krieger, M. A. (2011) Profiling the *Trypanosoma cruzi* phosphoproteome. *PLoS ONE* **6,** e25381
79. Treeck, M., Sanders, J. L., Elias, J. E., and Boothroyd, J. C. (2011) The Phosphoproteomes of *Plasmodium falciparum* and *Toxoplasma gondii* Reveal Unusual Adaptations Within and Beyond the Parasites' Boundaries. *Cell Host Microbe* **10,** 410–419
80. Mayank, P., Grossman, J., Wuest, S., Boisson-Dernier, A., Roschitzki, B., Nanni, P., Nühse, T., and Grossniklaus, U. (2012) Characterization of the phosphoproteome of mature Arabidopsis pollen. *Plant J.* **72,** 89–101